Theoretical models for T-stubs in contact with intermediate layer

M. Couchaux, M. Madhouni

Theoretical models for T-stubs in contact with intermediate layer

M. COUCHAUX[a], M. MADHOUNI[a]

[a] *Institut National des Sciences Appliquées de Rennes, 20 Avenue des Buttes de Coësmes, 35708, Rennes, France*

Abstract

During the last decade, simple solutions of thermal breaks have been developed for steel structures that consist in inserting an intermediate insulating layer (composed of PVC, plywood, elastomer, FRP…) between a bolted end-plate and a steel/concrete support. Experimental tests highlighted that failure modes under bending moment are similar to that of conventional bolted connections particularly in the tensile area, whereas the ultimate resistance decreases. For standard bolted connections loaded by a bending moment, the T-stub concept is used to model the tensile area. This model, extensively used in Eurocode 3, assumes that the end-plate is in contact with a rigid foundation or concrete/grout. T-stub can potentially be used to model the tensile area of bolted connections in presence of intermediate insulating layer. However the current model cannot be directly applied as the end-plate rests on a flexible support.

In the present paper, a mechanical model is proposed to firstly model the elastic behaviour of T-stubs in contact with a flexible intermediate layer. The model relies on the Timoshenko beam theory in contact with a Winkler foundation modelling respectively the end-plate and the intermediate layer. The contact pressure distribution being almost linear, simplifications are proposed in this sense. It is demonstrated that simplifications can be considered for standard material used as intermediate layer such as PVC or FRP. An analytical model is also given to calculate the ultimate resistance of T-stubs considering yielding of the intermediate layer. These results are validated by comparison to finite element analysis results performed with ANSYS code using solid and contact elements. This FE analysis highlights a clear distinction between the elastic and elasto-plastic behaviours of these T-stubs particularly concerning prying effects.

1. Introduction

The necessity to reduce heat loss of buildings and by consequence CO_2 emissions favor the development of innovative solutions for punctual thermal bridges in steel structures. A simple solution of punctual thermal bridge consists in placing an intermediate insulating layer between the steel/concrete support and the end-plate of a steel beam. Intermediate insulating layers can be composed of elastomer ([1], [2]), neoprene [3], Fiber-Reinforced Polymer ([8], [9], [10]), Fiber-Reinforced Resin [5], PVC ([2], [6], [7]) or plywood ([6], [7]). The mechanical behavior of this solution depends on the properties of the intermediate layer. Cleary et al [5] demonstrated experimentally that the insertion of FRR fillers reduce the stiffness of the connection by 10-20 %. The reduction of stiffness and ultimate resistance was more pronounced in presence of neoprene [3]. The crushing of the neoprene in the compressive area was very important and similar behaviour was observed during tests on connections with elastomer support [2]. The mechanical properties of elastomer were very low (see **Table 1**). Couchaux et al [6] performed experimental tests with intermediate layers stiffer than elastomer such as PVC and plywood (see Table 1). The failure mode corresponds to bolt failure in tension and the ultimate bending resistance decreased slightly in presence of extended end-plates. In the tensile area, Digital Image Correlation demonstrated that contact expanded in a large portion of the free edge of the end-plate in the tensile area when PVC or plywood were inserted. Peterman et al [10] demonstrated that FRP don't modify significantly the behaviour of the connection and don't yield in compression.

Table 1 : *Compressive properties of intermediate insulating layers*

Material	Elastic Modulus	Yield stress	Maximal Stress
	N/mm^2	N/mm^2	N/mm^2
Elastomer [2]	16,6	-	-
PVC [6]	200	4,4	-
Plywood [6]	302	6	-
FRR [5]	4210	-	289
FRP [10]	4270	-	411,7

The previous research's deal mainly with experimental tests, however accurate mechanical models are necessary to derive design methods. Nasdala et al [1] and Sulcova et al [4] proposed to adapt the component method of Eurocode 3 particularly for the evaluation of the behaviour of the compressive area. However, the mechanical characteristics of the tensile area was not particularly investigated. The use of intermediate insulating layers composed of various material necessitates to develop robust design methods to determine the stiffness and the resistance of the tensile area of this solution.

The T-stub concept is widely used to model the tensile area of bolted end-plate connections [11] and could be adapted to the proposed solution of thermal break. However the T-stub method assumes that the end-plate is in contact with a rigid foundation. These components are particularly impacted by prying forces. The prying force corresponds to the integral of the normal stress distribution over the contact zone and can significantly increase the bolt force. Extensive analytical studies on prying effects have been carried out by a number of researchers. For some time now, the prying force has been represented by a concentrated force acting at or near the end-plate edges of T-stubs ([11], [12], [13], [14]). In presence of a thin end-plate, this assumption can be inaccurate both in the elastic range of behavior [15] and at failure [16]. Kato & Tanaka [17] and Lemonis & Gantes [18] assumed a fixed support at the point of transition between the contact and the non-contact regions. At this point, the curvature is null and so is the bending moment. In the elastic range, the equilibrium position thus obtained is unique and depends on the ratio between the stiffness of the end-plate and the stiffness of the bolt. The hypothesis of concentrate force acting at or near the end-plate edge is acceptable for a relatively small contact area [15]. Senda et al. [19] proposed a linear distribution of the contact pressure, however Couchaux et al [15] demonstrated analytically and numerically that the contact pressure distribution may depend on the extent of the contact area and may not be unique in shape. Based on the refined beam theory of Baluch et al. [20], Couchaux et al [21] investigated the behaviour of prismatic solid in contact with a smooth rigid foundation and applied this model to determine the extent of the contact area of L-stubs and T-stubs in the elastic range

78 [15]. This approach was also applied to calculate the plastic and ultimate resistances of L-stubs
79 [16]. Recent papers have also been dedicated to refined calculation of the position of the prying
80 force of T-stubs in contact with rigid support. Qiang et al [22] used the energy method and
81 simple approximations to determine the position of the prying force in thin-walled T-stubs in an
82 iterative process. However, the contact pressure distribution was not evaluated. Hu et al [23]
83 considered the Timoshenko beam theory and the receding contact conditions but the contact
84 pressure distribution obtained was far from results of finite element analysis [15]. Katzeff [24]
85 also proposed a model considering Euler-Bernoulli beams resting on Winkler foundation and
86 thus neglects shear deformations.
87 The extent of the contact area can be particularly important in the tensile zone in presence of
88 flexible intermediate insulating layers such as PVC or plywood [6]. This aspect should thus be
89 investigated. Stiff intermediate layer, such as FRP, can significantly increase prying effects.
90
91 The main purpose of this paper is to propose an analytical model allowing the evaluation of
92 the mechanical characteristics of T-stubs in contact with intermediate insulating layers. These
93 components could be used to model moment resisting bolted end-plate connections. The
94 objective is to cover a large range of material from flexible one such as PVC, with Young
95 modulus around 200 N/mm^2 and yield strength of 5-10 N/mm^2, to stronger one such as FRP,
96 with Young modulus up to 20-30000 N/mm^2 and yield strength of 400-500 N/mm^2.
97 Firstly, non-linear finite element analysis has been performed with ANSYS using solid and
98 contact elements (see section 2). These simulations demonstrated that prying effects depend on
99 the compressive stiffness of the intermediate layers, particularly on the elastic range of
100 behaviour. On the contrary, prying effect is homogenised for the different materials at failure
101 and ultimate resistances are similar.
102

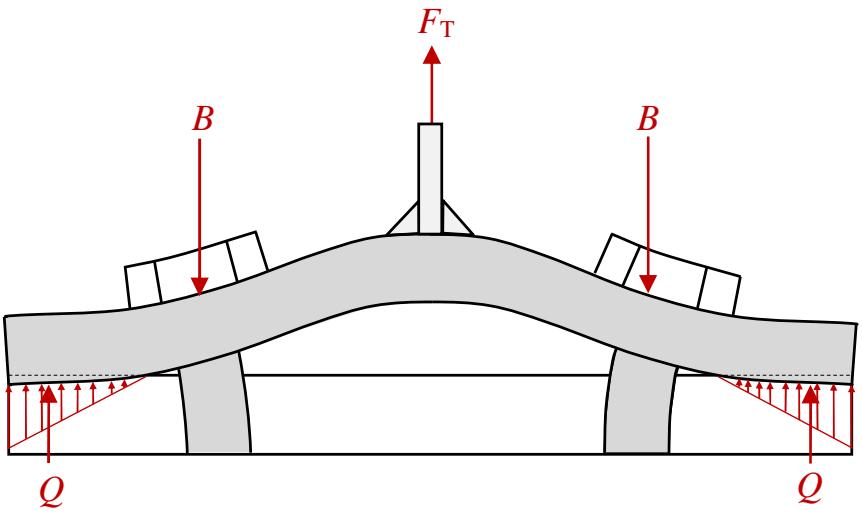

***Figure 1**: T-stub in tension in contact with a flexible intermediate layer*

An analytical model is proposed in section 3 to fully characterize the behaviour of T-stubs resting on intermediate layer, and particularly the force-displacement curve. As suggested in EN 1993-1-8, the force-displacement curve is built from two essential characteristics of the connection: the tensile resistance and the initial stiffness. These parameters are representative of the elastic and elasto-plastic ranges of behaviour. The elastic behaviour is modelled in section 3.1 considering Timoshenko beam theory for end-plates resting on Winkler foundation and maintained by an axial stiffener that corresponds to bolt action. The axial stiffness, bolt forces as well as the contact pressure distribution are determined with this model. Simplifications are also proposed assuming a linear distribution of the contact pressure. The ultimate resistance is derived in section 3.2. The ultimate resistance of T-stubs in contact with an intermediate layer is determined in section 3.2.1 taking into account the interaction with the support when bolt rupture in tension occurs. The length of the contact area is evaluated assuming a rectangular distribution of contact pressure. The ultimate resistance of T-stub in contact with a rigid support is then presented in paragraph 3.2.3. The ultimate resistance of flexible T-stubs involving end-plate failure is treated in paragraph 3.2.4 including influence of bolt bending. The results obtained via these analytical models are compared favourably against numerical predictions.

2. *Finite element analysis of T-stubs*

2.1. Presentation of the finite element model

The FE model developed with the finite element code ANSYS V19.0 was previously validated by comparison to experimental tests on L-stubs [16]. Components (bolts, end-plate and intermediate layer) are generated with three dimensional hexahedral elements (see Figure 2-b). For bolts, a constant cross-section equal to the effective cross-section area, A_s was used over the entire length. The threads are not modelled and continuity is assumed between the bolt shank and the nut. Only a quarter of the connection needs to be modelled due to symmetries (see Figure 2-a). The lower planes of the layer and the bolt are fixed.

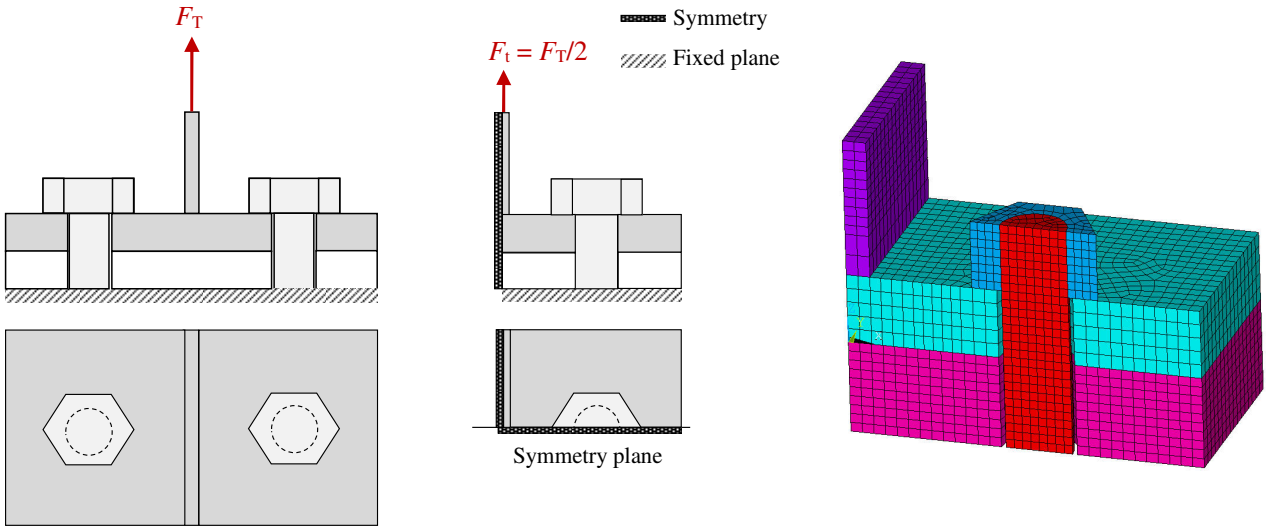

a) Symmetries b) Meshing

Figure 2 : *Symmetry and meshing of the numerical model*

Contact between the different components of the connections have been modelled considering sliding and sticking conditions with an isotropic Coulomb friction law with $\mu = 0{,}3$. Contact interaction has been included between bolt head and end-plate, end-plate and intermediate layer, bolt shank and end-plate/layers. A vertical displacement was uniformly applied at the top of the T-stub web. The mechanical behaviour of steel components (bolt, end-plate, web and weld) and intermediate layer has been defined according to an elastic-plastic behaviour with isotropic hardening. The von Mises criterion is used to model plastic yielding for steel and intermediate layer materials. Large deformations and displacements are taken into

account for all simulations. The stress-strain relationship has been defined using a multi-linear shape (see Figure 3). As soon as the deformation level reaches ε_u, the stress drops to 10 N/mm^2 in order to model the failure of the element. This simplification leads either to a drop-off of the force applied to the joint or to the termination of the calculation that is assumed to be the ultimate state of the joint. The accuracy of this model has been confirmed by comparison to experimental tests [16].

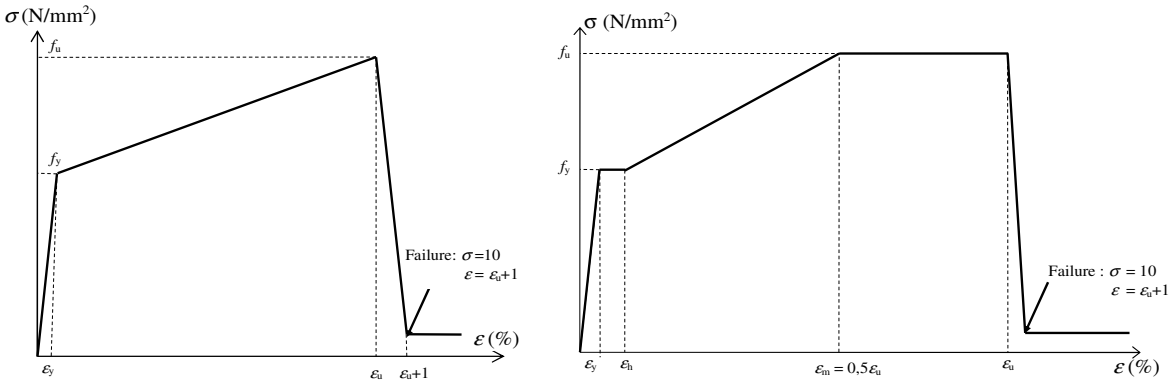

a) End-plate, intermediate layer b) Bolt

Figure 3 : *Stress-strain curves*

End-plate and web were composed of S355 steel, and bolts were of 10.9 class. The material properties adopted are listed in Table 2. For the elasto-plastic analysis depicted in section 2.2.2, three materials have been considered for intermediate layers:

- MAT-1 has very low stiffness and resistance with a Young's Modulus of 200 N/mm^2, yield and ultimate strengths are equal to 5 and 30 N/mm^2, respectively. This material is similar to PVC used by Couchaux et al [6] for tests on moment resisting connections.
- MAT-100 is similar to stiff FRP with a Young's Modulus of 25000 N/mm^2, yield and ultimate strengths are equal to 500 and 700 N/mm^2, respectively.
- MAT-10 is an intermediate solution between MAT-1 and MAT-100.

For elastic analysis presented in section 2.2.1, the Young's Modulus of intermediate insulating layer varies between 57 N/mm^2 and 100000 N/mm^2.

Table 2 : *Mechanical characteristics used for steel or intermediate layers*

Material	Element	E	f_y	ε_h	f_u	ε_u
		N/mm^2	N/mm^2	%	N/mm^2	%
Steel	End-plate/weld/web	210000	355	-	720	40
	Bolt	200000	900	1	1050	10
Intermediate layer	MAT-1	200	5	-	30	40
	MAT-10	2500	50	-	70	20
	MAT-100	25000	500	-	700	20

156

157 Six T-stub configurations have been studied varying the bolt diameter, intermediate layer
158 and end-plate thicknesses, as well as intermediate layer material (from MAT-1 to MAT-100).
159 The analyzed T-stub's geometries are presented in Table 3 and Figure 4.

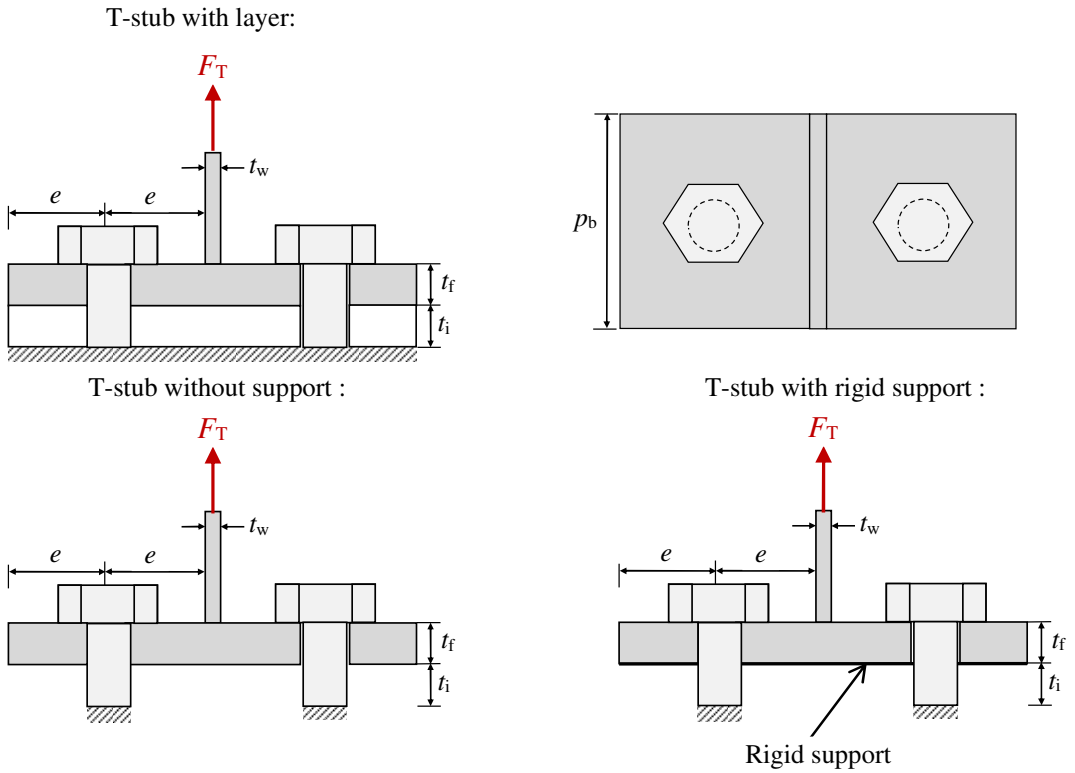

Figure 4 : *Configuration of T-stubs*

160 The web of the T-stub is welded to the end-plate by full penetration butt weld in order to
161 avoid any effect of the throat thickness in the case of fillet weld. The pitch and width of the six
162 connections are equal to 35 and 80 mm, respectively. The geometry of T1 and T2 is extracted
163 from bolted end-plate connections tested by Couchaux et al [6] with and without intermediate
164 insulating layer labelled PA-1 and RTPA-1-P/B. The thickness of the intermediate insulating

layer is the only difference between these two connections. A similar connection, T4, has been studied with an intermediate layer of 10 mm thickness. The analysis of T-stubs T1, T2 and T4 allows studying the impact of the intermediate layer thickness. The geometrical characteristics of connections T2, T5 and T6 are identical except the end-plate thickness which is equal to 15, 20 and 10 mm, respectively. The effect of the bolt diameter could be studied comparing the results of connections T2 and T3 that use bolts M16 and M20, respectively. In addition, each connection has been studied replacing the intermediate layer by a rigid plane or removing the intermediate layer. For T-stub T1, these connections are labelled T1-rigid and T1-flexible. The bolt length is identical for the three types of T-stubs (see Figure 4).

Table 3 : *Geometry of T-stubs studied*

Connection	t_p	e	p_b	t_i	t_w	Bolt
	mm	mm	mm	mm	mm	-
T1	15	35	80	30	10	M16
T2	15	35	80	20	10	M16
T3	15	35	80	20	10	M20
T4	15	35	80	10	10	M16
T5	20	35	80	20	10	M16
T6	10	35	80	20	10	M16

2.2. Numerical results

2.2.1. *Elastic behaviour*

Finite element analysis demonstrated that the extent of the contact area depends on the flexibility of the intermediate layer, which is directly related to its thickness and Young's Modulus. For a given geometry, the contact area increases with the decrease of the flexibility of the intermediate layer. A stiffer layer counterbalances the end-plate displacements caused by end-plate bending. The length of the contact area, e - ξ, evaluated in front of bolts (see Figure 6) is depicted in Figure 5 as a function of the Young's Modulus of the intermediate layer, E_i. The length of the contact area decreases with increasing value of the Young's Modulus and tends towards that obtained with a rigid support.

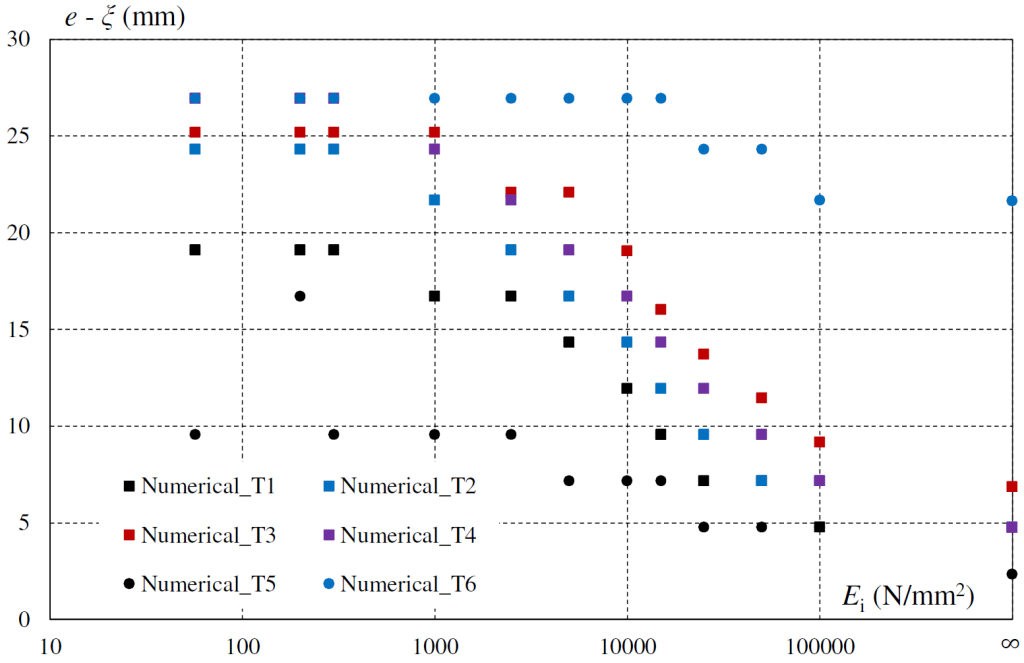

Figure 5 : *Evolution of the extent of the contact area in front of bolts*

For low values of the Young's Modulus, the contact area length decreases with the increase of intermediate layer thickness because bolt elongation increase and limits prying effect. T-stubs T1, T2 and T4 have similar geometries except the intermediate layer thickness. The length of the contact area of T1 is shorter than that of T2 and T4. For connection T3, using the larger bolt diameter, the extent of the contact area increases comparatively to other connections. This result is clearly in line with analysis of L-stubs and T-stubs resting in contact with a rigid support [6]. The increase of the end-plate thickness decreases the size of the contact area whatever the flexibility of the foundation. For connection T5, prying effects develop at the outer edge of the end-plate whatever the stiffness of the foundation. The end-plate is sufficiently rigid to limit its contact with the intermediate layer or the rigid support.

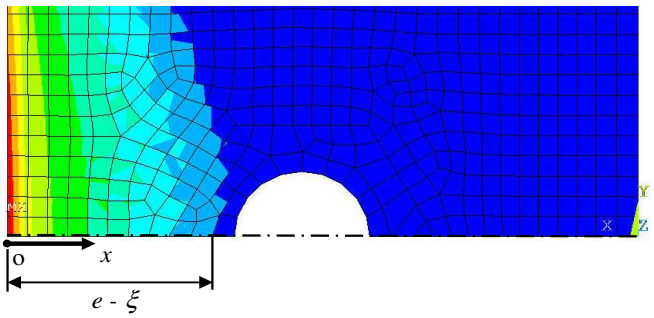

Figure 6 : *Contact pressure between the end-plate and the intermediate layer*

196 The shape of the contact pressure distribution evaluated from the outer edge of the end-plate
197 in the middle of the connection (see Figure 6) is presented in Figure 7. The connections were
198 loaded by a tensile force F_T equal to 20 kN and remained elastic. The contact pressure
199 distribution is almost linear with a local increase at the outer edge. The modification of the slope
200 of the contact pressure distribution at the outer edge is mainly related to the mesh density. For
201 MAT-100, the contact pressure distribution does not overlap with that obtained with a rigid
202 support, even if the stiffness and bolt force are almost identical. When the bolt diameter is
203 greater than the end-plate thickness, for connections T3 and T5, the contact area extends to the
204 bolt hole in presence of the most flexible intermediate layer, MAT-1. For connection T6, the
205 linearity is less clear, and a double curvature is obtained in presence of a rigid support. This
206 shape is in line with conclusions of the analytical model of Couchaux et al [15] for L-stubs and
207 T-stubs in contact with a rigid foundation.

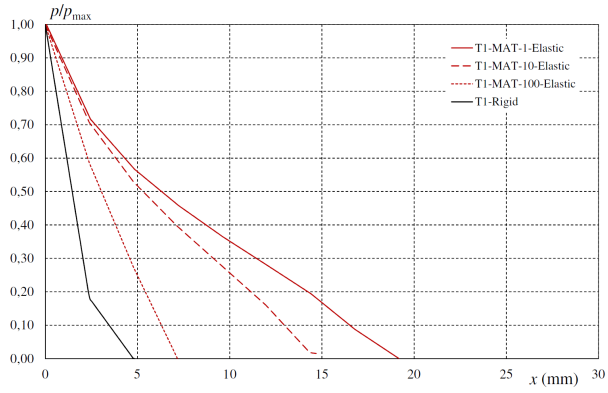

a) Connection T1

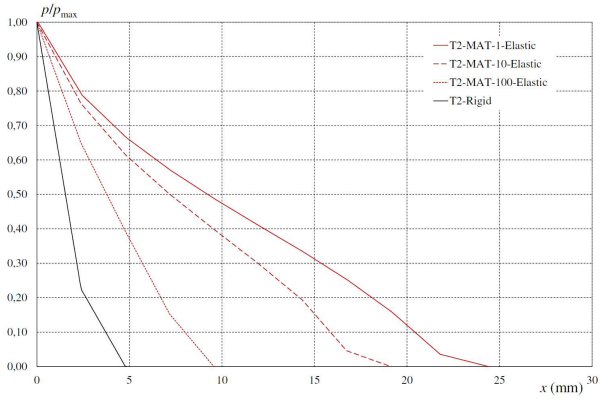

b) Connection T2

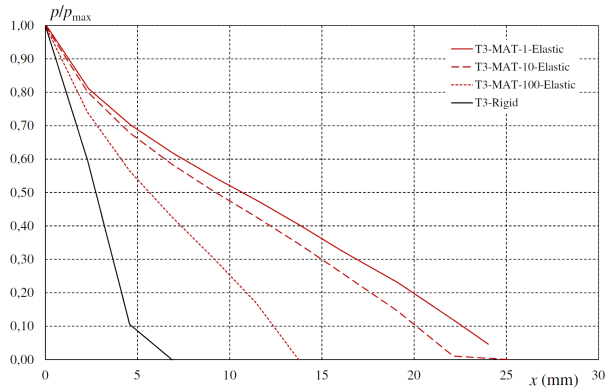

c) Connection T3

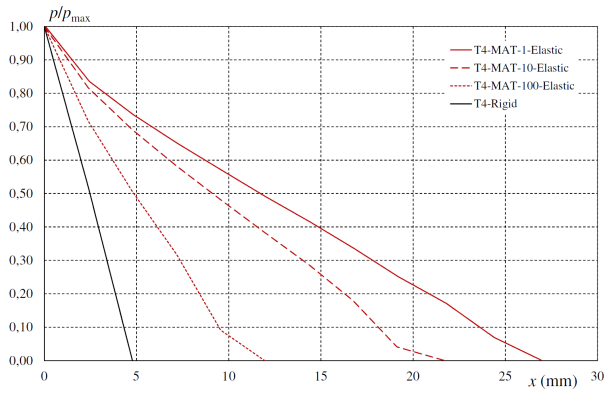

d) Connection T4

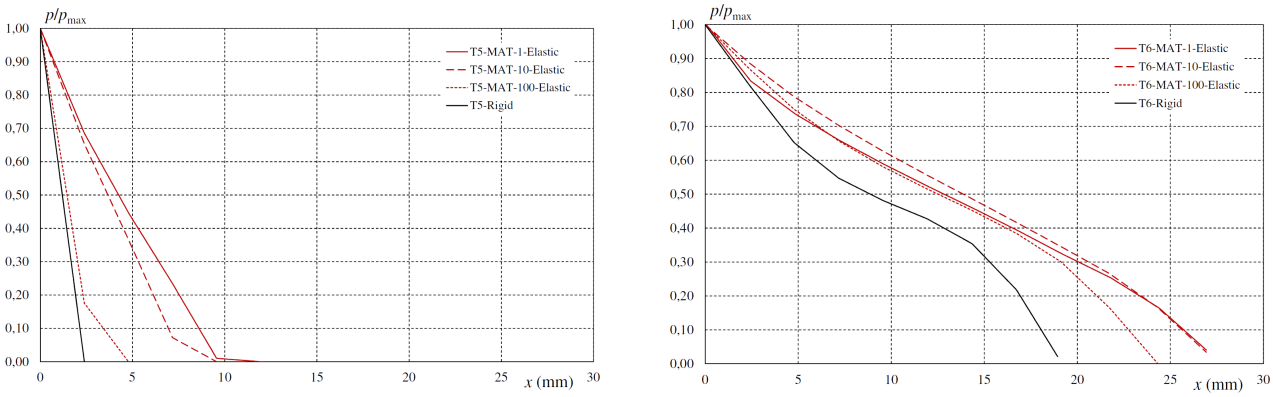

e) Connection T5 f) Connection T6

Figure 7 : *Shape of the contact pressure distribution*

The extents of the contact area and the contact pressure distribution are directly related to prying effect and particularly the bolt tensile force, B. The ratio of B to F_t, noted η, is presented in Figure 8 as a function of the Young's Modulus for the six connections. F_t is the tensile force applied to half a T-stub (see Figure 2). An increase of the layer stiffness results in an increase of the ratio η, and thus prying effect. Hence, the bolt force increases with increasing Young's Modulus of the layer.

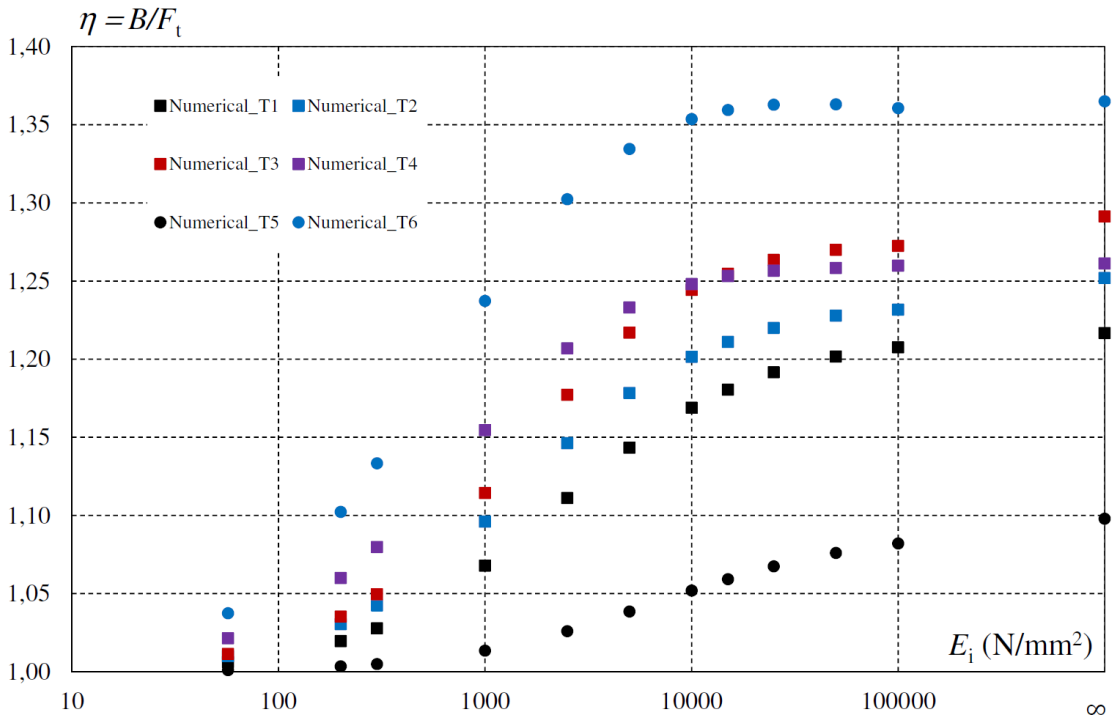

Figure 8 : *Evolution of the ratio* $\eta = B/F_t$

214 The ratio η tends to the value obtained with a T-stub resting on a rigid support. For a
215 Young's modulus of intermediate layer E_i equal to 25000 N/mm^2, equivalent to a stiff FRP
216 material, the difference is less than 3% for the six connections. These connections could thus be
217 analyzed as classical T-stubs in contact with a rigid support for the elastic range of behaviour.
218 On the contrary, for low values of E_i, the ratio η tend to 1 even if the extent of the contact is
219 significant (see Figure 7 for MAT-1). The layer is thus too flexible to develop substantial prying
220 forces. Prying action is nearly negligible for MAT-1. T-stubs T1, T2 and T4 have similar
221 geometry except the intermediate layer thickness respectively equal to 30, 20 and 10 mm. It can
222 be observed that prying effect is more preponderant for connection T4. The bolt being shorter,
223 its stiffness increases and thus the prying force.

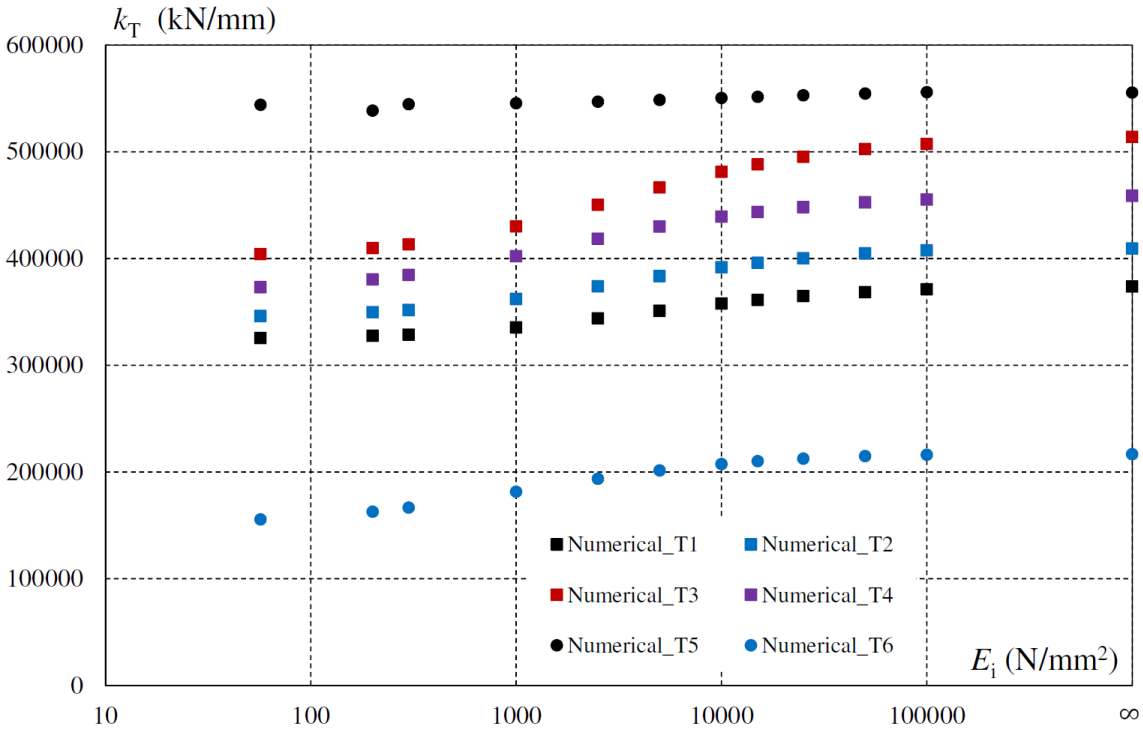

Figure 9 : *Evolution of the stiffness k_T*

224 Prying effect also increases with increasing bolt diameter. The ratio η is thus greater for
225 connection T3 comparatively to connections with identical end-plate thickness. The same
226 conclusion can be drawn when the end-plate thickness decreases. These results are in line with
227 conclusions made for L-stubs and T-stubs in contact with a rigid foundation [6]. For connection

T5, prying effect is slightly impacted by the evolution of the Young's Modulus, this phenomenon is limited even in presence of a rigid support.

The variation of prying effect also influences the stiffness of the T-stub. This latter is presented in Figure 9 as a function of the Young's modulus of layers for the six connections. An increase of the layer's stiffness increases the stiffness of the connection, that tends rather quickly to the value obtained for a T-stub in contact with a rigid foundation. When the Young's modulus of the layer is equal to 25000 N/mm^2, the difference with a T-stub in contact with a rigid support is less than 3.6%. The largest difference in term of stiffness between the softer layer and the rigid support is equal to 28%, for connection T6. With the most flexible layer, the stiffness is logically close to that obtained without layer. The stiffness increases with the decrease of the layer thickness. The increase of the bolt diameter and end-plate thickness increase the stiffness of the steel components and thus of the T-stub. For connection T5, the stiffness is constant whatever the value of the Young's Modulus because the prying force is quite limited together with penetration of the end-plate into the layer.

2.2.2. *Elasto-plastic behaviour*

The observed failure mode was bolt rupture in tension and bending for all connections. The addition of the three types of material did not affect the final failure mode. The conclusions of Couchaux et al [6] were similar for moment resisting beam-to-column bolted end-plate connections with intermediate layers composed of PVC or plywood. The ultimate resistances of the T-stubs are listed in Table 4.

For connections T1, T2, T4 and T5, the resistances obtained with intermediate layer are rather close to those with a rigid support. It is particularly true with materials MAT-10 and MAT-100. The resistances obtained with MAT-1 are generally lower than that obtained with a rigid support except for connection T5. For the latter, the prying effect is limited because of a thick end-plate. The ultimate resistance is thus not particularly influenced by the mechanical characteristics of the layer. For connection T3, the reduction of resistance obtained with MAT-1 is more pronounced comparatively to other T-stubs. Prying effect is in fact more significant due to a

greater stiffness of the bolts. As a result, the mechanical characteristics of the support influences the final response of the connection and particularly the ultimate resistance.

The resistance of T-stubs without support is clearly lower than that with intermediate layer or rigid support except for connection T5. These results may seem amazing because prying effect does not develop, and failure is caused by bolt rupture in tension. Nevertheless, the failure of the bolts is due to the combination of a tensile force and a bending moment. In presence of a flexible end-plate, that yields in bending, the rotations of the end-plate and the bolt are significant. The bending moment that develops on the bolt is thus substantial. For thick end-plate, the rotation is more limited and thus the bolt bending moment. The bolt tensile force can reach a value close to the pure bolt tensile resistance. Connection T5 develop nearly the same resistance whatever the presence or absence of a support. For this connection, the largest resistance is obtained with the flexible T-stub because of the lack of prying effect and the low bolt bending moment. The decrease of resistance obtained in presence of MAT-1 for T-stubs T3 and T6 is also due to the development of a significant bolt bending moment.

Table 4 : *Ultimate resistance of T-stubs*

Connection	Ultimate resistance (kN)				
	MAT-1	MAT-10	MAT-100	Rigid	Flexible
T1	209,6	223,7	223,8	223,6	179,5
T2	202,1	222,8	222,6	217,0	178,5
T3	231,4	296,7	309,8	300,5	227,3
T4	193,4	218,0	219,4	219,3	175,5
T5	274,8	271,6	270,3	267,7	276,0
T6	124,9	143,2	146,2	148,1	96,8

The evolution of the ratio η during the loading is presented in Figure 10 for the six connections. Whatever the connection studied, prying effect increases during loading as a result of the modification of the relative stiffness of the different components: bolt, end-plate and intermediate layer. For T-stubs in contact with a rigid foundation, it has been widely demonstrated ([12], [14], [15]) that prying effect increases when the bolt stiffness increases comparatively to the end-plate stiffness. For connections with intermediate layer, prying effect

277 growth is firstly caused by end-plate yielding in bending. It is followed by intermediate layer
278 yielding in compression that accentuates the phenomenon. Finally, bolts yield in tension and
279 bending. Consequently the stiffness of this component decreases reducing the prying effect.
280 However, the bolt force continues to increase up to rupture even if prying effect decreases. The
281 increase of prying effect during the elasto-plastic range of behavior is particularly pronounced
282 for the most flexible intermediate layer MAT-1. In this case, the ratio η does not exceed 1.10
283 during the elastic range of behavior but can reach values around 1.3 at failure except for
284 connection T5. Prying effects is thus nearly absent during the elastic stage but becomes
285 substantial at failure. We can notice that at failure the ratio η and thus the bolt force is lower for
286 the most flexible layer. However, the ultimate resistance is lower which may seem amazing
287 because failure is caused by bolt rupture in tension. This decrease is due to the significant
288 bending moment that develops together with a greater rotation of the end-plate which is not
289 reduced by the flexible support. For T1 and T2 configurations, the evolution of prying effect
290 until failure is similar (see Figure 10-a and b) as well as the ultimate resistance. The thickness of
291 the intermediate layer does not strongly influence the ultimate resistance and prying effect at
292 failure. For T3-configurations prying effects are very different at failure (see Figure 10-c). The
293 resistance of the first connection is also lower than that obtained with the three other
294 connections. The ratio between the bolt diameter and the end-plate thickness has a dominant
295 effect on the influence of intermediate layer stiffness on the final ultimate resistance. Prying
296 effect is very close for the four T4-configurations at failure (see Figure 10-d), and the ultimate
297 resistances are also very similar. This homogeneous response at failure is probably due to the
298 fact that the intermediate layer is thin, 10 mm, and by consequence the deformability of the
299 support is reduced in presence of a flexible material. For connection T5 (see Figure 10-e), even
300 if prying effect increases after yielding of end-plate and intermediate layer, the ratio η is limited
301 at failure (less than 1.15 for the four T5 configurations). This limitation of prying effect is due
302 to high rigidity of the end-plate. Contact area develops at the end-plate outer edge for the T5
303 configurations (see Figure 7-e).

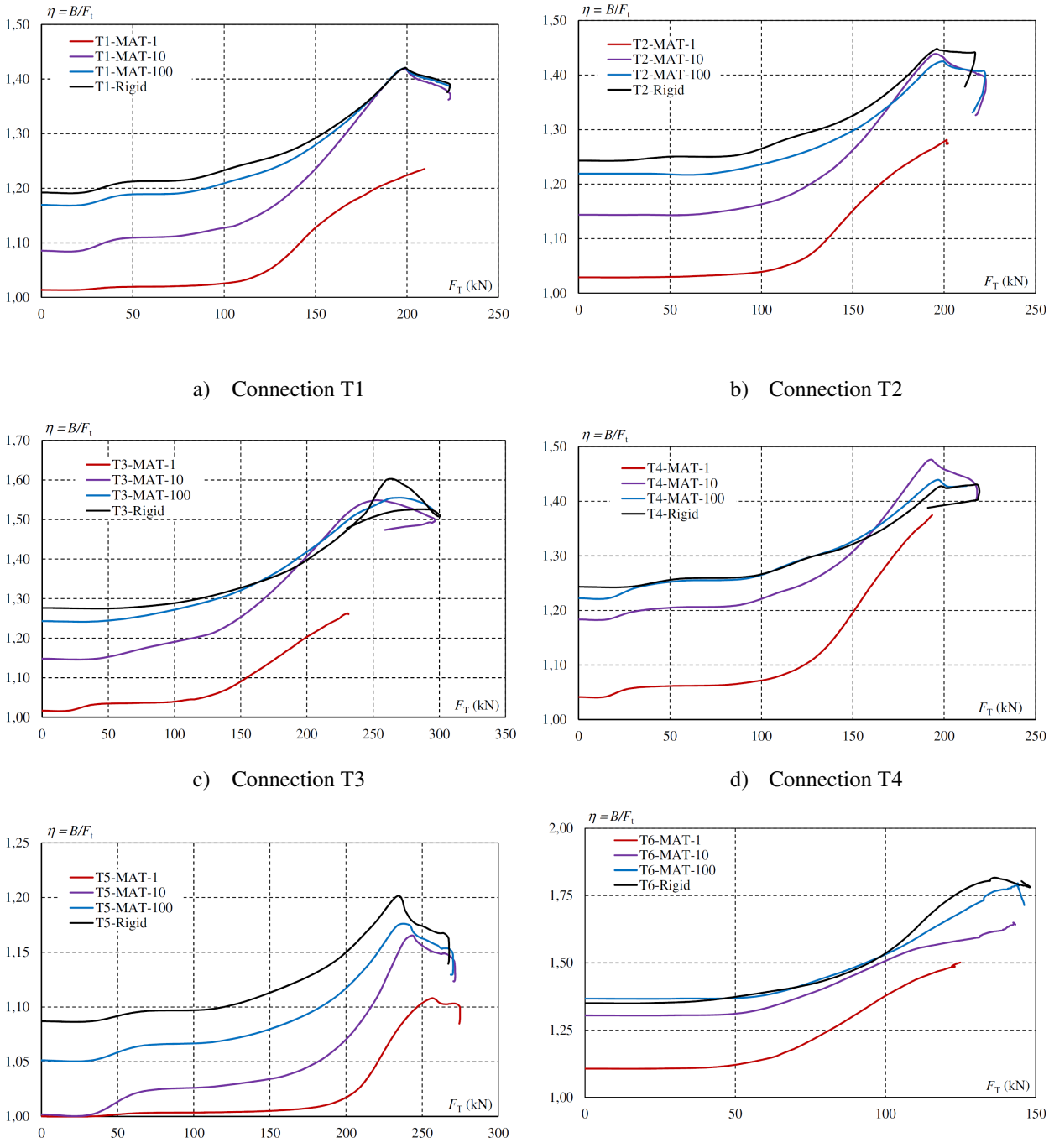

a) Connection T1

b) Connection T2

c) Connection T3

d) Connection T4

e) Connection T5

f) Connection T6

Figure 10 : *Evolution of the ratio η until failure*

The tensile force is depicted as a function of the connection's displacement in Figure 11. The connection's displacement is measured at the junction between the end-plate and the web. The force-displacement curves obtained with MAT-100 match very well with those of rigid T-stubs both in the elastic range of behavior (see also section 2.2.1) and in the elasto-plastic range of

behavior. In addition, the ultimate resistances of these connections are nearly identical. The behavior of T-stubs with MAT-10 is globally close to that obtained with a T-stub in contact with a rigid support even if yielding starts earlier.

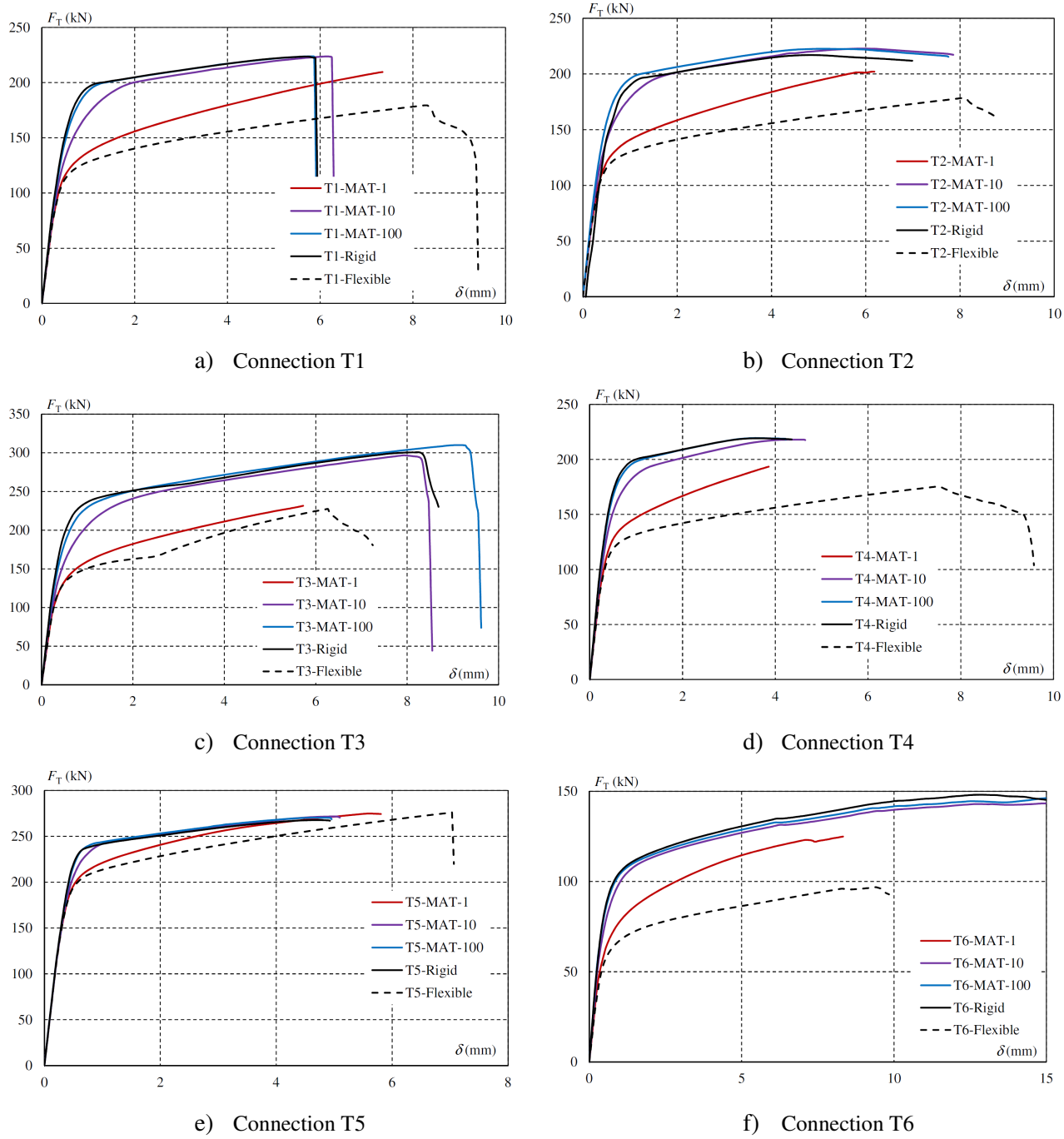

a) Connection T1

b) Connection T2

c) Connection T3

d) Connection T4

e) Connection T5

f) Connection T6

Figure 11 : *Force-displacement curves*

Yielding starts early as a result of lower mechanical properties of intermediate layer in compression comparatively to steel. However, the ultimate resistance is not strongly affected by the addition of this material. On the contrary, T-stubs with MAT-1 are clearly more flexible

than T-stubs in contact with a rigid support (see also Figure 9). The plastic resistance decreases as a consequence of an early yielding of the intermediate layer in compression and end-plate in bending. Despite this early yielding, the curve converges at failure (except for T3 and T6, see Figure 11-c and f), the ultimate resistance being rather similar. The curves obtained for the T5-configurations matched very well even with MAT-1 because the contact area is very limited. The force-displacement curves of flexible T-stubs are far from other ones except for connection T5. This difference is mainly due to an early yielding in bending of the end-plate and the bolt that is the consequence of the absence of support. When the end-plate is more rigid, for connection T5, the behavior of the five configurations is similar.

2.2.3. *Conclusions on the numerical simulations*

The main conclusions from the finite element analysis of the six T-stub connections are the following:

- For low values of the Youngs modulus of the intermediate layer (between 57 and 300 N/mm^2) that correspond to PVC and plywood tested by Couchaux et al [6], prying effect is very limited during the elastic range of behavior, the ratio η being lower than 1,1. These flexible supports are not able to develop substantial prying forces. In addition, the stiffness is on average 15% lower than that obtained for a T-stub in contact with a rigid support but very similar to stiffness of flexible T-stubs (without support).
- For material properties closer to a stiff FRP, with a Young's Modulus greater than 25000 N/mm^2, the elastic and elasto-plastic behaviors are very close to that obtained with a rigid T-stub whether for prying effect, stiffness or ultimate resistance.
- The final failure mode that corresponds to bolt rupture in tension and bending is not affected by the properties of the intermediate layer. However, for flexible intermediate layers and particularly MAT-1 (E_i = 200 N/mm^2 and f_{yi} = 5 N/mm^2) and flexible T-stubs, the bending of the bolt is more pronounced. The ultimate resistance is not influenced by the presence of intermediate layer when the bolt diameter is equal or

lower than the end-plate thickness. For bolt diameter greater than the end-plate thickness, the ultimate resistances of T-stubs with flexible intermediate layer (MAT-1 in particular) were 15-25 % lower than that with rigid support. This aspect should be considered for the development of future design methodologies.

- For intermediate material, MAT-10 in the present study, the elastic and elasto-plastic behaviors are similar to that obtained with rigid supports.
- In presence of intermediate layer, the contact pressure distribution is almost linear during the elastic range of behaviour.
- The effect of the mechanical properties of intermediate layer is limited for thick end-plate as the contact area is localized at the end-plate outer edge.

3. *Analytical models*

3.1. Elastic behaviour

3.1.1. *General assumptions*

A model based on the Timoshenko beam theory is used to evaluate the extent of the contact area, the deformation of the end-plate, the contact stress distribution and therefore the location of the prying force. The material is assumed to remain linear elastic. Due to the symmetrical geometry of the problem, the end-plate slope is zero at the web/end-plate junction (see Figure 12). The bolt is represented by a linear elastic spring. The stiffness of the bolt is defined according to EN 1993-1-8 rules:

$$k_b = \frac{EA_s}{L_b} \tag{1}$$

where L_b is the equivalent length of the bolt given in Table 6.11 of EN1993-1-8 [11], A_s the cross-section area of the bolt and E the Young's modulus of steel.

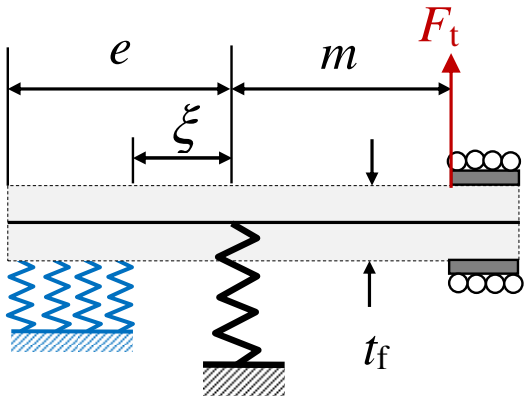

***Figure 12**: Model of an elastic T-stub in contact with a flexible intermediate layer*

The end-plate is subdivided in two parts: one portion is in contact with the flexible foundation and the other one is not (see Figure 12 and Figure 16). Both parts are modelled using the Timoshenko beam theory whose convention is presented in Figure 13.

In the non-contact area, which extend over the length $m + \xi$, the bending moment expression is thus:

$$M(x) = EI_{\mathrm{f}} \frac{d\phi(x)}{dx} \tag{2}$$

With:

I_{f} : Moment of inertia of the end-plate :

$$I_{\mathrm{f}} = \frac{l_{\mathrm{eff}} t_{\mathrm{f}}^3}{12} \tag{3}$$

l_{eff} : Effective length of the T-stub given by Eq. (6),

ϕ : rotation of the cross section:

$$\phi(x) = -\frac{dw(x)}{dx} + \frac{1}{GA_{\mathrm{f}}} \frac{dM(x)}{dx} \tag{4}$$

w: Transverse displacement of the end-plate,

G : Shear modulus of steel,

A_{f} : Reduced cross-section area for shear deformation :

$$A_{\mathrm{f}} = 0,8 t_{\mathrm{f}} l_{\mathrm{eff}} \tag{5}$$

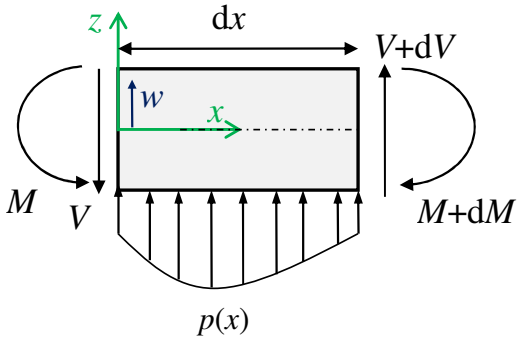

Figure 13: *Convention for beam modelling*

The effective length, l_{eff}, of the T-stub which corresponds to the cross-section width of the "beam" p_{b} (see Figure 4) is taken here as that proposed for T-stubs by Lemonis & Gantes [18]:

$$\frac{l_{\mathrm{eff}}}{p_{\mathrm{b}}} = \begin{cases} \dfrac{1}{0,92 + 0,06/(m/p_{\mathrm{b}})^2} & \text{if} \quad m/p_{\mathrm{b}} < 0,87 \\ 1 & \text{if} \quad m/p_{\mathrm{b}} \geq 0,87 \end{cases} \tag{6}$$

Over the contact area, the beam rests on Winkler foundation, the lateral displacement is thus related to the contact pressure distribution:

$$p(x) = -k_c w(x) \tag{7}$$

Where k_c is the stiffness of the Winkler foundation:

$$k_c = \frac{E_i l_{eff}}{t_i} \tag{8}$$

With:

E_i : Young modulus of the intermediate layer.

The relation between the bending moment and the contact pressure distribution being:

$$p(x) = -\frac{d^2 M(x)}{dx^2} \tag{9}$$

Inserting Equations (7) and (9) in (2), we get the typical differential equation for Timoshenko beam resting on Winkler foundation:

$$\frac{d^4 w(x)}{dx^4} - 2\alpha_0 \frac{d^2 w(x)}{dx^2} + \beta_0 w(x) = 0 \tag{10}$$

With:

$$\alpha_0 = \frac{k_c}{2GA_f},\ \beta_0 = \frac{k_c}{EI_f}.$$

An identical equation can be expressed as a function of the bending moment inserting Equations (7) and (9) in (2):

$$\frac{d^4 M(x)}{dx^4} - 2\alpha_0 \frac{d^2 M(x)}{dx^2} + \beta_0 M(x) = 0 \tag{11}$$

This equation is identical to that proposed by Couchaux et al [15] for beam in contact with a rigid foundation.

393 3.1.2. *Behaviour in the contact area*

394 Considering only the portion of the end-plate in contact, the loading comprises (see Figure
395 14) the contact pressure distribution p, a bending moment M_0, and a shear force Q equal to the
396 prying force. Both M_0 and Q are applied at the point of transition between the contact and non-
397 contact regions (see Figure 14). At this point, the cross-section is allowed to rotate, i.e. no
398 kinematic constraints are imposed.

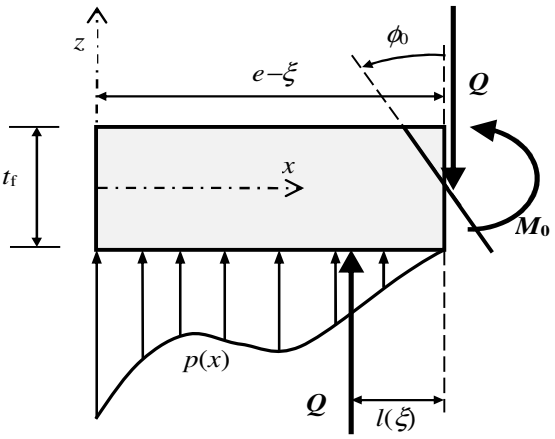

Figure 14 : *Area of the end-plate in contact*

399 The prying force Q can be computed by integrating the contact pressure distribution over the
400 contact area:

$$Q = \int_0^{e-\xi} p(x)dx \tag{12}$$

401 From Figure 14, it can be seen that the lever arm (distance to the inner boundary of the
402 contact zone) of the prying force is equal to the ratio M_0/Q:

$$l(\xi) = \frac{M_0}{Q} \tag{13}$$

403

404

405

406

407

408 The boundary conditions for the bending moment and the shear force are (see Figure 14):

$$\begin{aligned} &M(0)=0 \\ &\frac{dM}{dx}(0)=0 \\ &M(e-\xi)=-M_0,\ M_0\geq 0 \\ &\frac{dM}{dx}(e-\xi)=-Q,\ \ Q\geq 0 \end{aligned} \tag{14}$$

409 At the inner boundary of the contact area (located at $x = e - \xi$), the contact stress and thus
410 the contact pressure distributions are equal to zero:

$$p(e-\xi)=-\left.\frac{d^2M}{dx^2}\right|_{x=e-\xi}=0 \tag{15}$$

411 The bending moment distribution, solution of equation (11), has the following expression:

$$M(x)=-M_0e^{-a_0x}\left[\left(C_1\cos(b_0x)+C_2\sin(b_0x)\right)+e^{a_0x}\left(C_3\cos(b_0x)+C_4\sin(b_0x)\right)\right] \tag{16}$$

412 With:

$$a_0=\sqrt[4]{\beta_0}\cos\left[\frac{\arccos}{2}\left(\frac{\alpha_0}{\sqrt{\beta_0}}\right)\right],\ b_0=\sqrt[4]{\beta_0}\sin\left[\frac{\arccos}{2}\left(\frac{\alpha_0}{\sqrt{\beta_0}}\right)\right] \tag{17}$$

413 The four constants of integration C_i are evaluated via the boundary conditions (14) and (15),
414 their expressions are given in appendix A.1. Taking the derivative of Eq. (14) gives the shear
415 force or equivalently the prying force. Therefore the distance $l(\xi)$ between the prying force and
416 the point of transition between the contact and non-contact regions can be evaluated via
417 equation (13) to give:

$$l(\xi)=\frac{1}{e^{-a_0(e-\xi)}\left[b_0\mu_1(e-\xi)-a_0\varphi_1(e-\xi)\right]+e^{a_0(e-\xi)}\left[a_0\varphi_3(e-\xi)+b_0\mu_3(e-\xi)\right]} \tag{18}$$

418 Where:

$$\varphi_i(e-\xi)=C_i(e-\xi)\cos\left[b_0(e-\xi)\right]+C_{i+1}(e-\xi)\sin\left[b_0(e-\xi)\right] \tag{19}$$

$$\mu_i(e-\xi)=C_{i+1}(e-\xi)\cos\left[b_0(e-\xi)\right]-C_i(e-\xi)\sin\left[b_0(e-\xi)\right] \tag{20}$$

419 The ratio of the contact pressure and its maximum value is presented in Figure 15 for
420 different values of E_i considering end-plate and intermediate layer thicknesses equal to 15 and

421 20 mm, respectively. The length of the contact area is fixed at 35 mm. For Young's modulus
422 lower than 2000 MPa, the contact pressure distribution is almost linear. For greater values, the
423 contact pressure distribution is non-linear. However, in a T-stub the contact area will decrease
424 and linear contact pressure distribution will be obtained (see section 2.2.1 and Figure 17).

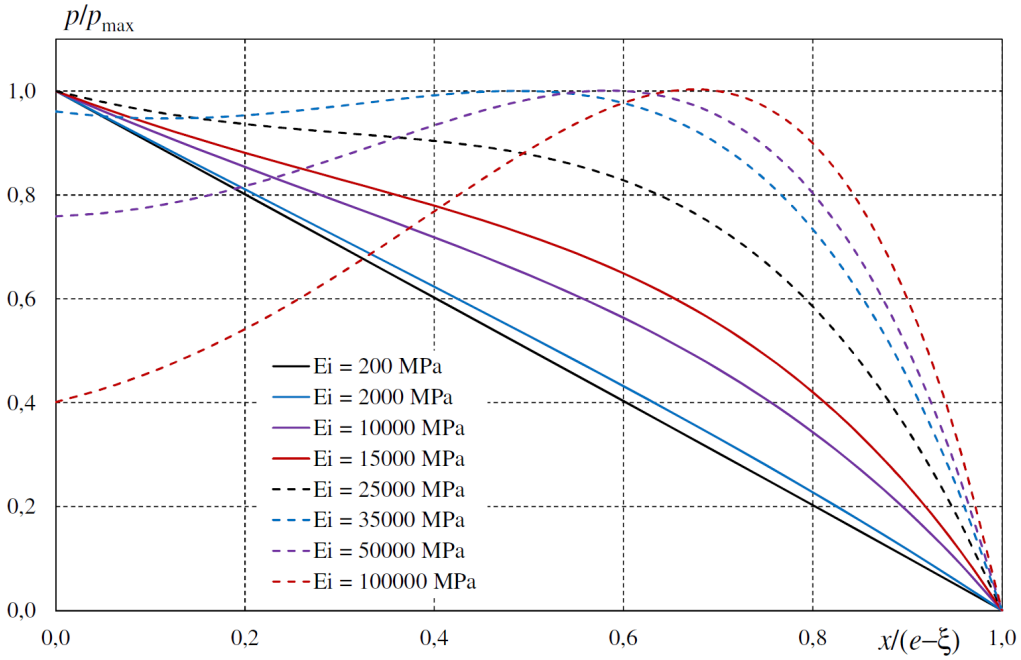

Figure 15 : *Shape of the contact pressure distribution*

425 The rotation at the uplift point is thus:

$$\phi(x=e-\xi)=\phi_0=\frac{1}{k_c}\frac{d^3M(e-\xi)}{dx^3}+\frac{1}{GA_f}\frac{dM(e-\xi)}{dx} \tag{21}$$

426 Finite element analysis demonstrated that the shape of the contact pressure distribution is
427 almost linear for the T-stubs studied. The analytical model developed in the present section
428 tends to the same conclusion for the configurations studied (see section 3.1.2). In the present
429 section, the shape of contact pressure distribution is directly assumed linear, and thus:

$$p(x)=p_{max}\left(1-\frac{x}{e-\xi}\right) \tag{22}$$

430 With:

431 p_{max}: Largest contact pressure occurring at the outer edge of the end-plate.

The prying force and lever arm become:

$$Q = \int_0^{e-\xi} p(x)dx = p_{\max}\frac{e-\xi}{2} \tag{23}$$

$$l(\xi) = \frac{2(e-\xi)}{3} \tag{24}$$

The maximal contact pressure distribution is related to the displacement at the outer edge $\delta_{\max}$ by:

$$p_{\max} = k_c \delta_{\max} \tag{25}$$

By compatibility, the global rotation of end-plate can be expressed as:

$$\phi_0 = \frac{\delta_{\max}}{e-\xi} \tag{26}$$

Inserting Eqs. (23) to (25) and (13) in (26), one obtains the relation between the rotation and the bending moment at the uplift point:

$$\phi_0 = \frac{3M_0}{k_c(e-\xi)^3} \tag{27}$$

The rotational stiffness is finally:

$$k_{\theta_0} = \frac{k_c}{3}(e-\xi)^3 \tag{28}$$

3.1.3. *Behaviour in the uplift area*

The second part of the flange lifts off from the foundation. The separation length ξ will be calculated assuming equilibrium of the lift-off part of the end-plate and the continuity of the stress-resultants at the point of transition between the contact and non-contact regions. The overall equilibrium conditions of lift-off portion of the end-plate produce the following equations:

$$Q = B - F_t \tag{29}$$

$$M_0 = F_t(m+\xi) - B\xi - M_E \tag{30}$$

The bending moment M_0 can also be expressed in the following manner:

$$M_0 = l(\xi)Q = l(\xi)\left(B - F_t\right) \tag{31}$$

446 Inserting Eqs (29) and (31) into (30) gives the bolt force:

$$B = \frac{F_t(m+n) - M_E}{n} \tag{32}$$

447 Where n is the distance between the location of the prying force and the bolt axis:

$$n = \xi + l(\xi) \tag{33}$$

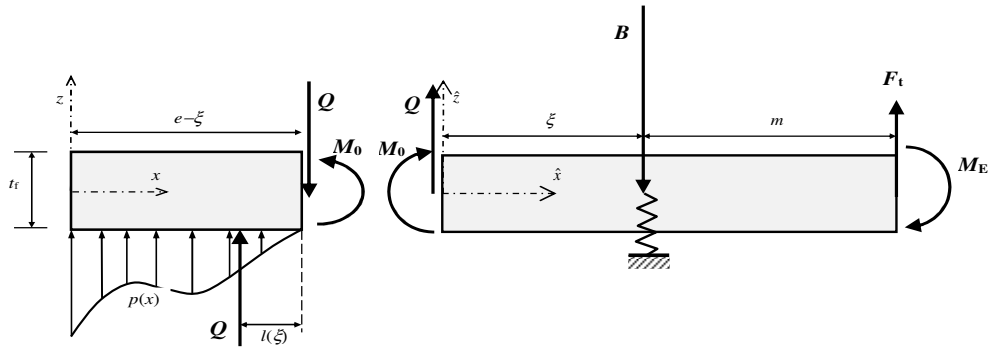

Figure 16 : *Modelling in contact and uplift areas*

448 The contact pressure distribution p being equal to zero in the non-contact region and since no
449 external distributed loading is applied to the flange, the relationship between the bending
450 moment and the transverse displacement is given simply by:

$$M(\hat{x}) = -EI_f \frac{d^2 w(\hat{x})}{d\hat{x}^2} \tag{34}$$

451 For $0 \le \hat{x} \le \xi$, we have the following expression for the bending moment:

$$M(\hat{x}) = -F_t(m + \xi - \hat{x}) + B(\xi - \hat{x}) + M_E \tag{35}$$

452 The transverse displacement is equal to zero at $\hat{x} = 0$ but the rotation is obtained considering
453 the continuity with the contact area:

$$\phi(\hat{x} = 0) = \phi(x = e - \xi) = \frac{1}{k_c}\frac{d^3 M(e-\xi)}{dx^3} + \frac{1}{GA_f}\frac{dM(e-\xi)}{dx} \tag{36}$$

454 That can be expressed as a function of the bending moment at the uplift point:

$$\phi(\hat{x} = 0) = \phi_0 = \frac{M_0}{k_{\theta_0}} \tag{37}$$

455 Inserting Eq (35) into (34), integrating twice the outcome and making use of the above
456 mentioned boundary conditions, we obtain the following expression for the deflection of the
457 beam centreline at the bolt axis:

$$w(\xi) = F_{\mathrm{t}}\delta_{\mathrm{F}} - B\delta_{\mathrm{B}} - M_{\mathrm{E}}\delta_{\mathrm{M_E}} \tag{38}$$

458 Where:

$$\delta_{\mathrm{F}} = \frac{\xi^2(m/2+\xi/3)}{EI_{\mathrm{f}}} + \frac{\xi}{GA_{\mathrm{f}}} + \frac{\xi(m+\xi)}{k_{\theta_0}},$$

459
$$\delta_{\mathrm{B}} = \frac{\xi^3}{3EI_{\mathrm{f}}} + \frac{\xi}{GA_{\mathrm{f}}} + \frac{\xi^2}{k_{\theta_0}},$$

$$\delta_{\mathrm{M_E}} = \frac{\xi^2}{2EI_{\mathrm{f}}} + \frac{\xi}{k_{\theta_0}}.$$

460 Due to symmetry of T-stubs, the rotation at $\hat{x} = \xi + m$ can be written as:

$$\phi(\xi+m) = -\Theta_{\mathrm{F}}F_{\mathrm{t}} + \Theta_{\mathrm{B}}B + \Theta_{\mathrm{M_E}}M_{\mathrm{E}} = 0 \tag{39}$$

461 Where:

$$\Theta_{\mathrm{M_E}} = \frac{\xi+m}{EI_{\mathrm{f}}} + \frac{1}{k_{\theta_0}},$$

462
$$\Theta_{\mathrm{B}} = \frac{\xi^2}{2EI_{\mathrm{f}}} + \frac{\xi}{k_{\theta_0}},$$

$$\Theta_{\mathrm{F}} = \frac{(\xi+m)^2}{2EI_{\mathrm{f}}} + \frac{\xi+m}{k_{\theta_0}}.$$

463 Thus, we get the following expression of the bending moment M_{E}:

$$M_{\mathrm{E}} = -m_{\mathrm{B}}B + m_{\mathrm{F}}F_{\mathrm{t}} \tag{40}$$

464 Where:

465
$$m_{\mathrm{B}} = \frac{\Theta_{\mathrm{B}}}{\Theta_{\mathrm{M_E}}},\quad m_{\mathrm{F}} = \frac{\Theta_{\mathrm{F}}}{\Theta_{\mathrm{M_E}}}.$$

466 Combining relations (32) and (40), we obtain the equation relating the bolt force B to the
467 external force applied F_{t}:

$$B = \frac{m+n-m_{\mathrm{F}}}{n-m_{\mathrm{B}}}F_{\mathrm{t}} = \eta F_{\mathrm{t}} \tag{41}$$

468 Expressing that the elongation of the bolt is equal to the transverse displacement at the bolt
469 location, one obtains:

$$\frac{B}{k_b} = F_t\delta_F - B\delta_B - M_E\delta_{M_E} \tag{42}$$

470 Inserting Eqs (40) and (41) in the above equation, we get:

$$g(\xi) = (m+n-m_F)\left(\frac{1}{k_b} + \delta_B - \delta_{M_E} m_B\right) - (n-m_B)(\delta_F - \delta_{M_E} m_F) = 0 \tag{43}$$

471 Equation (43) of $g(\xi)$ allows the determination of the separation length ξ and thus the extent
472 of the contact area. This equation is non-linear and may be solved numerically. The calculation
473 of the bolt force can be done using Equation (41). The size of the contact area, given by the
474 value of ξ, lies within the interval [0, e]. It is worth mentioning that ξ does not depend on the
475 magnitude of the applied force F_t. A similar result was also obtained for T-stub in contact with a
476 rigid foundation [15]. Eq (43) can be simplified considering a linear distribution of contact
477 pressure distribution using the rotational stiffness given by Eq (28) and neglecting shear
478 deformation to:

$$a_1\xi + b_1\xi^2 + c_1\xi^3 + d_1\xi^4 + v_1\xi^5 + h_1 = 0 \tag{44}$$

479 With

$$a_1 = \frac{EI_f}{2}\left(\frac{2}{3}e^3k_c - e.m^2k_c - m^2e.k_c - m^2k_b\right)$$

$$b_1 = \frac{k_cEI_f}{4}\left(m^2 - \frac{m^2e^3k_b}{3EI_f} - 3e^2\right)$$

480 $$c_1 = \frac{k_cEI_f}{24}\left(5\frac{m^2e^2k_b}{EI_f} + 12e + 4m\right)$$

$$d_1 = \frac{k_c}{12}\left(-2m^2ek_b - EI_f\right),$$

$$v_1 = \frac{m^2k_ck_b}{24},$$

$$h_1 = \frac{EI_f}{4}\left(m^2e^2k_c + \frac{4}{3}me^3k_c + EI_f\right).$$

481 The last equation allows to determine the separation length ξ and all the other unknowns of
482 the problem depending on this variable.

483 3.1.4. *Axial stiffness*

484 Using the continuity in displacement and rotation at the bolt location, one obtains the
485 maximum displacement:

$$w(m+\xi)=\delta_{\mathrm{t}}=F_{\mathrm{t}}\left[\frac{(m+\xi)^3}{3EI_{\mathrm{f}}}+\frac{m+\xi}{GA_{\mathrm{f}}}\right]-B\left[\frac{\xi^2}{EI_{\mathrm{f}}}\left(\frac{\xi}{3}+\frac{m}{2}\right)+\frac{\xi}{GA_{\mathrm{f}}}\right]-M_{\mathrm{E}}\frac{(m+\xi)^2}{2EI_{\mathrm{f}}}+\phi_0(m+\xi) \tag{45}$$

486 Inserting Equations (31), (37) and (40) in (45), we get:

$$\delta_{\mathrm{t}}=F_{\mathrm{t}}\left\{\begin{array}{l}\dfrac{1}{6EI_{\mathrm{f}}}\left[2(m+\xi)^3-\eta\xi^2(2\xi+3m)-3(m_{\mathrm{F}}-m_{\mathrm{B}}\eta)(m+\xi)^2\right]\\ +\dfrac{1}{GA_{\mathrm{f}}}\left[m+(1-\eta)\xi\right]+\dfrac{l(\xi)(\eta-1)(m+\xi)}{k_{\theta_0}}\end{array}\right\} \tag{46}$$

487 The axial stiffness is finally:

$$k_{\mathrm{t}}=\frac{1}{\dfrac{1}{k_{\mathrm{tf}}}+\dfrac{1}{k_{\mathrm{tv}}}+\dfrac{1}{k_{\mathrm{t}\theta_0}}} \tag{47}$$

488 With:

$$k_{\mathrm{tf}}=\frac{6EI_{\mathrm{f}}}{2(m+\xi)^3-\eta\xi^2(2\xi+3m)-3(m_{\mathrm{F}}-m_{\mathrm{B}}\eta)(m+\xi)^2},$$

489
$$k_{\mathrm{tv}}=\frac{GA_{\mathrm{f}}}{m+(1-\eta)\xi},$$

$$k_{\mathrm{t}\theta_0}=\frac{k_{\theta_0}}{l(\xi)(\eta-1)(m+\xi)}.$$

490 In absence of intermediate layer, for flexible T-stubs, the axial stiffness is simply:

$$k_{\mathrm{t0}}=\frac{1}{\dfrac{1}{k_{\mathrm{tf0}}}+\dfrac{1}{k_{\mathrm{tv0}}}+\dfrac{1}{k_{\mathrm{b}}}} \tag{48}$$

491 With:

$$k_{\mathrm{tf0}} = \frac{3EI_{\mathrm{f}}}{m^3},$$

$$k_{\mathrm{tv0}} = \frac{GA_{\mathrm{f}}}{m}.$$

3.1.5. *Comparison with numerical simulations*

The prying factors, η, evaluated with the analytical and numerical models are presented in Table 5 for different values of the Young Modulus of the layer. The contact pressure distribution has been assumed linear, because the difference with the more complex analytical model accounting for the non-linear distribution of the contact pressure, does not exceed 0,6 %. The results are in good agreements between the analytical and numerical models, with an error less than 7,5 %. The analytical approach generally overestimates the prying factor giving a conservative estimation of the bolt force. The difference between the two models is more pronounced when the end-plate thickness is lower than the bolt diameter, for T-stubs T3 and T6. The model could be improved considering the flexibility of bolt in bending. The analytical model is able to capture the increase of prying effects with increase of the Young Modulus of the layer.

Table 5 : *Ration η calculated analytically and numerically*

T-stub	T1		T2		T3		T4		T5		T6	
E_{i} (N/mm^2)	η_{ana}	η_{num}	η_{ana}	η_{num}	η_{ana}	η_{num}	η_{ana}	η_{num}	η_{ana}	η_{num}	η_{ana}	η_{num}
57	1,01	1,01	1,01	1,01	1,01	1,01	1,02	1,02	1,00	1,00	1,05	1,04
200	1,02	1,02	1,03	1,03	1,04	1,04	1,07	1,06	1,00	1,00	1,14	1,10
300	1,03	1,03	1,05	1,04	1,06	1,05	1,09	1,08	1,01	1,00	1,19	1,13
1000	1,07	1,07	1,11	1,10	1,14	1,11	1,19	1,15	1,02	1,01	1,33	1,24
2500	1,13	1,11	1,17	1,15	1,22	1,18	1,24	1,21	1,03	1,03	1,39	1,30
5000	1,16	1,14	1,21	1,18	1,26	1,22	1,27	1,23	1,04	1,04	1,41	1,33
10000	1,19	1,17	1,23	1,20	1,29	1,24	1,28	1,25	1,06	1,05	1,41	1,35
15000	1,20	1,18	1,24	1,21	1,29	1,25	1,28	1,25	1,07	1,06	1,41	1,36
25000	1,21	1,19	1,25	1,22	1,30	1,26	1,28	1,26	1,08	1,07	1,40	1,36
50000	1,22	1,20	1,25	1,23	1,30	1,27	1,29	1,26	1,09	1,08	1,39	1,36
100000	1,23	1,21	1,26	1,23	1,30	1,27	1,28	1,26	1,09	1,08	1,39	1,36

The axial stiffness evaluated with the analytical and numerical models are presented in Table 6 for different values of the Young's Modulus of the layer. The results are also in good

agreement between the two approaches. The analytical model generally overestimates the stiffness but the error remains lower than 10 %. For Young's Modulus lower than 1000 N/mm^2, the initial stiffness is close to the stiffness calculated analytically without support (for E_i = 0 N/mm^2 in Table 6).

Table 6 : *Axial stiffness calculated analytically and numerically*

T-stub	T1		T2		T3		T4		T5		T6	
E_i	$k_{t,ana}$	$k_{t,num}$	$k_{t,ana}$	$k_{t,num}$	$k_{t,ana}$	$k_{t,num}$	$k_{t,ana}$	$k_{t,num}$	$k_{t,ana}$	$k_{t,num}$	$k_{t,ana}$	$k_{t,num}$
N/mm^2	kN/mm	kN/mm	kN/mm	kN/mm	kN/mm	kN/mm	kN/mm	kN/mm	kN/mm	kN/mm	kN/mm	kN/mm
0	339	324	357	344	387	404	378	369	579	544	137	152
57	340	325	359	346	390	404	383	373	580	544	143	156
200	342	328	364	350	397	410	394	380	580	539	155	163
300	343	329	366	352	401	413	400	384	580	545	162	167
1000	351	335	380	362	425	430	428	402	581	545	191	182
2500	361	344	396	374	452	450	451	419	583	547	212	194
5000	370	351	409	383	473	467	465	430	585	548	222	202
10000	378	358	419	392	489	481	476	439	587	550	228	207
15000	382	361	423	396	497	488	480	443	588	552	230	210
25000	387	365	428	400	504	495	485	448	590	553	232	213
50000	391	368	433	405	511	502	489	453	591	554	232	215
100000	395	371	437	408	516	507	492	455	593	556	233	216

The proposed analytical model is able to determine with a good accuracy two important parameters that characterized T-stubs loaded in tension, the axial stiffness and the bolt force. This model could thus be used to evaluate the initial rotational stiffness of moment resisting connections using intermediate layer.

The shape of the contact pressure distribution of connections T3 and T6 evaluated with the full analytical model is presented in Figure 17 for MAT-1, MAT-10 and MAT-100. The finite element analysis highlighted that these T-stubs developed the largest contact area. For connection T3, the contact pressure distribution is linear whatever the intermediate layer. For connection T6, the shape of the contact pressure is slightly non-linear for MAT-10 and MAT-100. This non-linearity is caused by the increase of the contact area and the decrease of the end-plate thickness. The assumption of a linear contact pressure is thus completely justified.

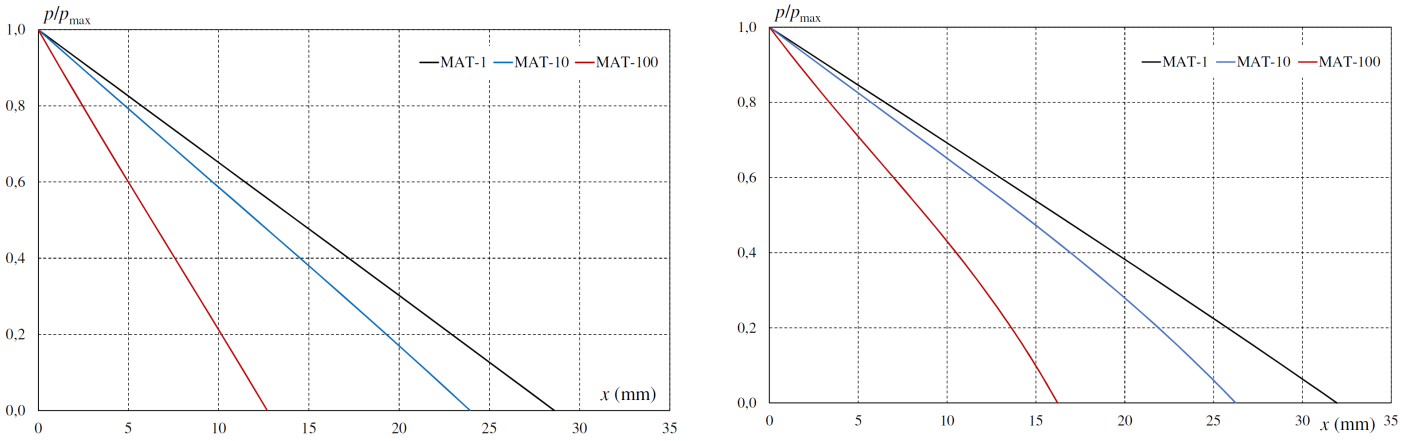

a) Connection T3 b) Connection T6

Figure 17 : *Contact pressure distribution evaluated with the full analytical model*

3.2. Ultimate tensile resistance

3.2.1. *Failure modes*

For T-stubs in contact with a rigid support or an intermediate layer, three failure modes involving the end-plate and bolts are considered:

- **Mode 1:** End-plate failure mechanism with prying effect (see Figure 18-a),
- **Mode 2:** Bolt rupture with prying effect (see Figure 18-b),
- **Mode 3:** Bolt rupture without prying effect (see Figure 18-c).

These failure modes are in line with assumptions of Eurocode 3 part 1-8 [11]. The resistances corresponding to failure modes 1 and 3 are identical whatever the contact condition and are directly presented in this section. For mode 2, the prying effect will depend on the support and will be depicted in section 3.2.2 and 3.2.3 for T-stubs in contact with intermediate layer and rigid supports, respectively.

The tensile force which leads to the failure of yield lines on the end-plate in presence of prying effect is:

$$F_{\mathrm{T,1,u}} = \frac{4M_{\mathrm{u,f}}}{m} \tag{49}$$

With

$M_{\mathrm{u,f}}$: Ultimate bending moment that develop on the end-plate:

542 $$M_{u,f} = \frac{l_{eff} f_{m,f} t_f^2}{4}$$

543 $f_{m,f}$: Medium ultimate strength that develop on the end-plate proposed by Packer [26] :

544 $$f_{m,f} = \frac{f_{y,f} + 2 f_{u,f}}{3}$$

545 $f_{y,f}$: End-plate yield strength,

546 $f_{u,f}$: End-plate ultimate tensile strength.

547

548 The effective length, l_{eff}, is equal to the width of the T-stub in the present study.

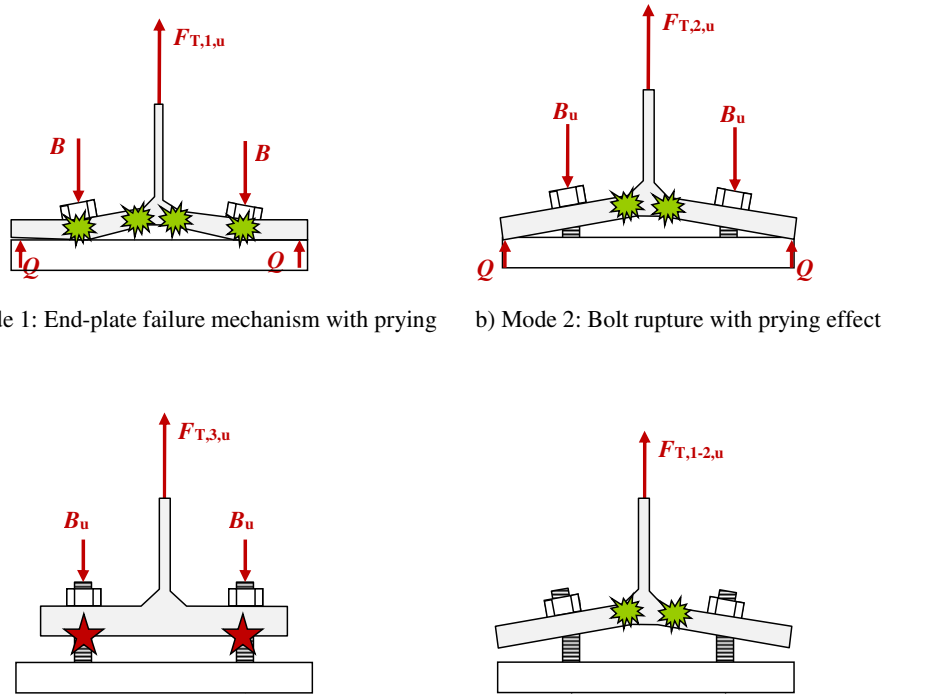

a) Mode 1: End-plate failure mechanism with prying

b) Mode 2: Bolt rupture with prying effect

c) Mode 3: Bolt rupture without prying

d) Mode 1-2: End-plate mechanism without prying

Figure 18 : *Failure modes of T-stubs in tension*

549 For mode 3, the resistance corresponds to the sum of bolt tensile resistances:

$$F_{T,3,u} = 2B_u \qquad (50)$$

550 With :

551 B_u: Bolt tensile resistance:

552 $$B_u = 0{,}9 A_s f_{ub}$$

553 f_{ub}: Ultimate bolt tensile strength,

554 A_s: Bolt cross section area.

555

556 The tensile resistance of T-stub is taken as the smallest of the values for the three failure
557 modes:

$$F_{T,u} = \min\left(F_{T,1,u};\ F_{T,2,u};\ F_{T,3,u}\right) \tag{51}$$

558

559

560 For T-stubs not in contact with a support, labeled flexible T-stub in this paper, two failure
561 modes are possible:

562 - **Mode 1-2:** End-plate failure mechanism without prying effect (see Figure 18-
563 d),
564 - **Mode 3:** Bolt rupture without prying effect (see Figure 18-c).

565 The tensile resistance of failure mode 1-2 includes bolt bending that can be non-negligible in
566 presence of thin end-plates. This resistance is derived in section 3.2.4.

567 3.2.2. *Bolt failure of T-stubs in contact with an intermediate layer*

568 At failure the contact pressure distribution is assumed to reach the ultimate compressive
569 strength of the layer labelled f_{ui} (see Figure 19). The ultimate resistance of the bolt in tension,
570 B_u, is reached, as well as the ultimate bending resistance of the end-plate, $M_{u,f}$.
571 The axial equilibrium gives:

$$F_{T,2,u} / 2 = B_u - Q \tag{52}$$

572 With :

573 Q: Prying force that can be expressed as

$$Q = l_{eff}\,(e - \xi_u)\,f_{ui} \tag{53}$$

574 f_{ui}: ultimate compressive strength of the intermediate layer.

575

576

577 One obtains with the bending moment equilibrium:

$$F_{T,2,u}\left(m+\xi_u\right)/2-B_u\xi_u-M_{u,f}=Q\frac{e-\xi_u}{2} \tag{54}$$

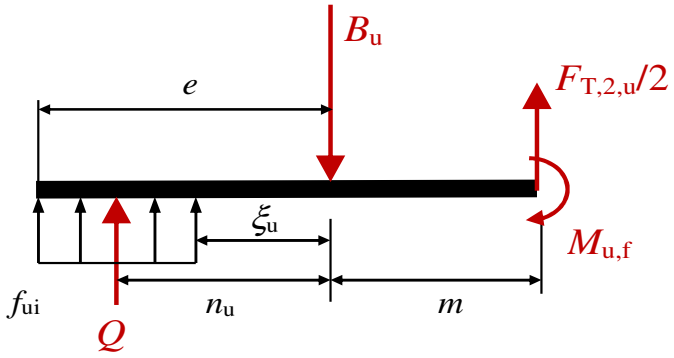

Figure 19 : *Bolt failure of half a T-stub in contact with an intermediate layer*

578 Inserting Eqs (52) and (53) in (54), we get the following quadratic equation:

$$\frac{\overline{X}^2}{2}-\alpha_R\overline{X}+\beta_R=0 \tag{55}$$

579 With:

580 $$\overline{X}=\frac{e-\xi_u}{e}$$

581 $$\alpha_R=\frac{e+m}{e}$$

582 $$\beta_R=\frac{B_u m-M_{u,f}}{l_{eff}f_{u,i}e^2}$$

583 The positive solution of this equation is:

$$\overline{X}=\alpha_R\left(1-\sqrt{1-2\frac{\beta_R}{\alpha_R{}^2}}\right) \tag{56}$$

584 The separation length is finally:

$$\xi_u=e\left[1-\alpha_R\left(1-\sqrt{1-2\frac{\beta_R}{\alpha_R{}^2}}\right)\right] \tag{57}$$

585 The ultimate tensile resistance of failure mode 2 can be expressed in the following manner:

$$F_{T,2,u}=\frac{2M_{u,f}+2n_uB_u}{m+n_u} \tag{58}$$

586 With:

587 n_u : Distance between the bolt axis and the point of application of the lever arm :

$$n_u = \frac{e + \xi_u}{2} \tag{59}$$

588 3.2.3. *T-stub in contact with a rigid support*

589 For T-stubs in contact with a rigid support, the ultimate tensile resistance is evaluated by the
590 following expression based on Eurocode 3:

$$F_{T,2,u} = \frac{2M_{u,f} + 2nB_u}{m+n} \tag{60}$$

591 With:

592 $n = \min\left(e;\ 1{,}25m\right)$

593 3.2.4. *Flexible T-stub*

594 In absence of prying effect, the failure mechanism corresponds to the development of a yield
595 line on the end-plate and a plastic hinge on the bolt (see Figure 20). The ultimate resistance is
596 thus:

$$F_{T,1\text{-}2,u} = \frac{2M_{u,f} + 2M_{u,b}}{m} \tag{61}$$

597 Where :

598 $M_{u,b}$: Ultimate bending moment of the bolt depending on the bolt tensile force :

$$M_{u,b} = M_{u,b,0}\left[1 - \left(\frac{B}{B_{u0}}\right)^2\right] \tag{62}$$

599 $M_{u,b,0}$: Ultimate bending moment of the bolt in absence of axial force:

$$M_{u,b,0} = W_{pl,b} f_{ub} \tag{63}$$

600 $W_{pl,b}$: Bolt plastic modulus.

601 B : Bolt tensile force.

602 B_{u0} : Ultimate tensile resistance of the bolt in absence of bending moment:

$$B_{u0} = A_s f_{ub} \tag{64}$$

603

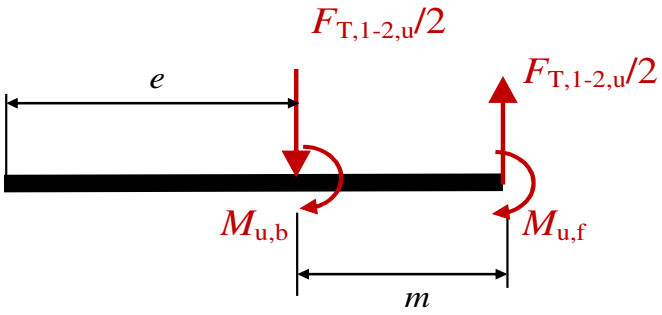

Figure 20 : *End-plate and bolt failures in bending of half a T-stub without support*

In absence of prying effect, the bolt force is equal to half the applied tensile force ($B = F_{T,1\text{-}2,u}/2$) and thus one obtains the ultimate resistance of the T-stub:

$$F_{T,1\text{-}2,u} = \chi_{1-2} F_{T,1\text{-}2,u,0} = \chi_{1-2} \frac{2M_{u,f} + 2M_{u,b,0}}{m} \tag{65}$$

With :

$$\chi_{1-2} = \frac{\sqrt{4f+1}-1}{2f}$$

$$f = \frac{M_{u,b,0} F_{T,1\text{-}2,u,0}}{2mB_{u0}^{\ 2}}$$

3.2.5. *Comparison with numerical simulations*

The ultimate tensile resistances calculated via the proposed analytical model have been compared against the predictions of the numerical model (see section 2.2.2) and are presented in Table 7. The results are in very good agreements whatever the T-stub configuration studied. The mean value of $F_{T,u,ana}/F_{T,u,num}$ is equal to 0,99. The analytical model is able to capture the increase of resistance caused by improvement of ultimate strength of the foundation. The analytical resistance is generally underestimated for flexible T-stubs. One can observe that the analytical model is not able to capture the reduction of resistance when the intermediate layer thickness increases mainly because the cinematic compatibility and strain hardening are neglected.

620 ***Table 7 :*** *Ultimate tensile resistance calculated analytically and numerically*

T-stub	T1		T2		T3		T4		T5		T6	
	$F_{T,u,ana}$	$F_{T,u,num}$	$F_{T,u,ana}$	$F_{T,u,num}$	$F_{T,u,ana}$	$F_{T,u,num}$	$F_{T,u,ana}$	$F_{T,u,num}$	$F_{T,u,ana}$	$F_{T,u,num}$	$F_{T,u,ana}$	$F_{T,u,num}$
	kN	kN	kN	kN	kN	kN	kN	kN	kN	kN	kN	kN
Flexible	172,6	179,5	172,6	178,5	197,8	227,3	172,6	175,5	279,2	276,0	92,9	96,8
MAT-1	210,5	209,6	210,5	202,1	233,1	231,4	210,5	193,4	278,0	274,8	136,8	124,9
MAT-10	215,3	223,7	215,3	222,8	281,1	296,7	215,3	218,0	278,0	271,6	136,8	143,2
MAT-100	218,0	223,8	218,0	222,6	296,1	309,8	218,0	219,4	278,1	270,3	136,8	146,2
Rigid	218,2	223,6	218,2	217,0	297,4	300,5	218,2	219,3	282,6	267,7	136,8	148,1

621 ## *4. Conclusion*

622 During the last decades, much attention has been paid to thermal breaks for steel structures
623 inserting intermediate insulating layers between bolted end-plate connections and steel/concrete
624 supports. For moment resisting connections, the flexibility of the intermediate layer is a key
625 aspect even in the compressive area but also in the tensile ones. For conventional bolted end-
626 plate connections, the tensile area is generally modelled considering T-stubs in contact or not
627 with a rigid support. This concept cannot be directly applied when the end-plate is in contact
628 with a flexible support. The main objective of this paper was to evaluate the elastic and elasto-
629 plastic behaviour of T-stubs in contact with intermediate insulating layers typically used in
630 moment resisting thermal breaks. A finite element model has firstly been developed in ANSYS
631 to simulate the behaviour of these components including contact elements, plasticity and great
632 displacements/strains. Six T-stubs have been studied varying the end-plate and intermediate
633 layer thicknesses, bolt diameter and material properties of the intermediate layer. These analyses
634 permit to establish first conclusions on the behaviour of T-stubs with a flexible intermediate
635 layer:

636 • During the elastic range of behaviour prying effect is very limited in presence of
637 flexible layer particularly when the Young's Modulus is less than 300 N/mm^2. These
638 layers correspond to PVC and plywood tested by Couchaux et al [6]. For these
639 configurations, the stiffness is very close to the stiffness obtained without support.
640 However, when components such as end-plate in bending and layer in compression
641 start to yield, the prying factor increases and prying effect becomes significant.

642 - For stiffer layers, with Young's Modulus greater than 25000 N/mm^2, the elastic
643 characteristics (prying factor and axial stiffness) are rather close to that obtained
644 with a T-stub in contact with a rigid support. These mechanical properties are similar
645 to that of stiff FRP. The ultimate resistances are also similar to that of T-stubs in
646 contact with a rigid support.
647 - The contact pressure distribution of T-stubs studied was almost linear during the
648 elastic range of behaviour whatever the mechanical properties of the layers studied.
649 The contact area increases with the decrease of the stiffness of the support.
650 - The failure mode that corresponds to bolt rupture loaded in tension and bending was
651 not affected by the properties of layers. However, the ultimate resistance generally
652 decreases with the reduction of mechanical properties of the layer. Particularly
653 when the end-plate thickness is lower than the bolt diameter.
654 - The mechanical properties of the layer do not influence the behaviour of T-stubs that
655 use thick end-plates because the contact area due to prying effect is very limited.

656 Based on the conclusions drawn from these numerical simulations, an analytical model has
657 been proposed to determine key parameters of T-stubs, the elastic stiffness and the ultimate
658 tensile resistance. A Timoshenko beam model resting on Winkler foundations has been
659 proposed to model T-stubs in contact with intermediate layers. This model confirmed that the
660 length of the contact area is independent from the magnitude of the external force and that the
661 contact pressure distribution is almost linear whatever the stiffness of the intermediate layer.
662 The separation length could thus be simplified to a 5th degree polynomial. This model permits to
663 evaluate with a good accuracy the prying factor and the axial stiffness. Finally, the ultimate
664 tensile resistance has been calculated considering that failure modes occur on the end-plate or
665 the bolts. The Eurocode 3 approach was adopted particularly for failure modes 1 et 3. However,
666 for mode 2 (bolt rupture with prying effect) of T-stubs in contact with a layer, prying forces
667 were evaluated assuming a uniform distribution of the compressive resistance of the layer. For
668 T-stubs without support the resistance of failure mode 1-2, corresponding to the development of

669 a plastic mechanism, was enriched adding the bending resistance of bolts non-negligible in
670 presence of thin end-plate.

671 This theoretical analysis should be confronted to experimental tests on T-stubs loaded in
672 tension varying the material of intermediate layers. In particular the anisotropy of the material,
673 not considered in the present study, may probably influence the behaviour of these components.
674 In addition, simplifications should be proposed for the evaluation of the elastic mechanical
675 properties.

676

677 ## *5. References*

678 [1] Nasdala L., Hohn B., Rühl R., Design of end-plate connections with elastomeric
679 intermediate layer, Journal of Constructional Steel Research, Vol. 63, p. 494-504, 2007.

680 [2] Ben Larbi A., Couchaux M., Bouchaïr A., Thermal and mechanical analysis of thermal
681 break with end-plate for attached steel structures, Engineering Structures, Vol. 131, p.
682 362-379, 2017.

683 [3] Hamel S., White S., Thermo-mechanical modelling and testing of thermal breaks in
684 structural steel point transmittances, Anchorage, AK, 2016.

685 [4] Sulcova Z., Sokol Z., Wald F., Structural connections with thermal separation, CESB 07
686 Prague Conference, p. 672-677, 2007.

687 [5] Cleary D.B., Riddell W.T., Camishion N., Downey P., Marko S., Neville G., Oostdyk M.,
688 Panaro T., Steel connections with fiber-reinforced resin thermal barrier filler plates under
689 service loading, Journal of Structural Engineering, Vol. 142, Issue 11, 2016.

690 [6] Couchaux M., Alhasawi A., Ben Larbi A., Monotonic and cyclic tests on beam to column
691 bolted connections with thermal insulation layer, Engineering Structures, Vol. 204,
692 109621, 2020.

693 [7] Ben Larbi A., Couchaux M., Thauvoye C., Sautot C., Mechanical and fire tests on
694 thermal breaks attached to concrete supports, Journal of Constructional Steel Research,
695 Accepted under proof, 2022.

696 [8] Peterman K.D., Moradei J., D'Aloisio J., Webster M., Hajjar J.F., The behaviour of
697 double lap splice bolted connections with Fiber-Reinforced Polymer fills, Workshop
698 Connection VIII, Boston, May 2016.

[9] K. D. Peterman, J. A. Kordas, J. Moradei, K. Coleman, J. A. D'Aloisio, M. D. Webster, and J. F. Hajjar, "Thermal Break Strategies for Cladding Systems in Building Structures: Report to the Charles Pankow Foundation," Boston, MA, 2016.

[10] Peterman K.D., Kordas J., Webster M.D., D'Aloisio J.A., Hajjar J.F., Structural performance of axially and laterally loaded cantilevers with thermally-improved detailing, Journal of Constructional Steel Research, Vol. 181, 106617, 2021.

[11] EN 1993-1-8: Eurocode 3 (May 2005): Design of steel structures – Part 1–8: Designs of joints.

[12] Jaspart J.P., Etude de la semi-rigidité des nœuds poutre-colonne et son influence sur la résistance et la stabilité des ossatures en acier, Thèse de doctorat en science appliquée, Université de Liège, 1990 (in French).

[13] Piluso V., Faella C., Rizzano G., Ultimate Behavior of Bolted T-stubs II : Model Validation, Journal of Structural Engineering, Vol. 127, Issue 6, p. 694-703, 2001.

[14] Girao Coehlo A.M., Characterization of ductility of bolted end plate beam-to-column steel connections, PhD dissertation, University of Coimbra, July 2004.

[15] Couchaux M., Hjiaj M., Ryan I., Bureau A., Effect of contact on the elastic behaviour of tensile bolted connections, Journal of Constructional Steel Research, Vol. 133, p. 459-474, 2017.

[16] Couchaux M., Hjiaj M., Ryan I., Bureau A., Tensile resistances of L-stubs, Journal of Constructional Steel Research, Vol. 138, p. 131-149, 2017.

[17] Kato, B., Tanaka, A. (1968), Experimental study on tension-type high strength bolted connection (No.2 Prying Action), Transaction of the architectural institute of Japan, Vol. 72, Issue 147, p. 33-41 (in Japanese).

[18] Lemonis, M.E., Gantes, C.J. (2006), Incremental modelling of T-stub connections, Journal of Mechanics of materials and structures, Vol. 1, Issue 7, p. 1135-1157.

[19] Senda, H., Suzuki, T., Ogawa, T. (1996), Inelastic behaviour of bolted T-stub connections, Journal of structural and construction engineering, Transaction of AIJ, Issue 476, p. 159-168 (in Japanese).

[20] Baluch, M.H., Azad, A.K., Khidir, M.A., (1984), Technical Theory of Beams with normal strain, Journal of Engineering Mechanics, Vol. 110, Issue 8, p. 1233-1237.

[21] Couchaux M., Hjiaj M., Ryan I., (2015), Enriched beam model for slender prismatic solids in contact with a rigid foundation, International Journal of Mechanical Sciences, Vol. 93, p. 181-190.

[22] Qiang X., Shen Y., Jiang X., Bijlaard F.S.K., Theoretical study on initial stiffness of thin-walled steel T-stubs taking account of prying force, Thin-Walled Structures, Vol. 155, 2020, 106944.

[23] Hu D., Papadopoulos J., Adams G.G., Prying action in an elastic T-stub tensile connection, Journal of Constructional Steel Research, Vol. 169, 2020, 106027.

[24] Katzeff S.E., An investigation into prying models in tension clips, Thin-Walled Structures, Vol. 145, 2019, 106398.

[25] Ahlasawi A., Couchaux M., INSA report, TREPOS-005-A, Numerical studies − thermal break attached to a steel support, 2018 (in French).

[26] Packer J., Bruno L., Birkemoe P., Limit analysis of bolted RHS flange plate joints, Journal of Structural Engineering, Vol. 115, p. 2226-2242, 1989.

745 ***Appendix A.1: Coefficients C_i***

746 $$C_1(\varsigma)=\frac{e^{a_0\varsigma}}{2}\frac{a_0^2\sin(b_0\varsigma)-2a_0b_0\cos(b_0\varsigma)-b_0^2\sin(b_0\varsigma)+(e^{a_0\varsigma})^2\left(-a_0^2\sin(b_0\varsigma)-2a_0b_0\cos(b_0\varsigma)+b_0^2\sin(b_0\varsigma)\right)}{a_0\left((e^{a_0\varsigma})^4b_0-4a_0\sin(b_0\varsigma)\cos(b_0\varsigma)(e^{a_0\varsigma})^2-b_0\right)}$$

747 $$C_2(\varsigma)=-\frac{e^{a_0\varsigma}}{2}\frac{a_0^2\cos(b_0\varsigma)b_0+2a_0b_0^2\sin(b_0\varsigma)-b_0^3\cos(b_0\varsigma)+(e^{a_0\varsigma})^2\left(2a_0^3\sin(b_0\varsigma)+3a_0^2b_0\cos(b_0\varsigma)+b_0^3\cos(b_0\varsigma)\right)}{a_0b_0\left((e^{a_0\varsigma})^4b_0-4a_0\sin(b_0\varsigma)\cos(b_0\varsigma)(e^{a_0\varsigma})^2-b_0\right)}$$

748 $$C_3(\varsigma)=-\frac{e^{a_0\varsigma}}{2}\frac{a_0^2\sin(b_0\varsigma)-2a_0b_0\cos(b_0\varsigma)-b_0^2\sin(b_0\varsigma)+(e^{a_0\varsigma})^2\left(-a_0^2\sin(b_0\varsigma)-2a_0b_0\cos(b_0\varsigma)+b_0^2\sin(b_0\varsigma)\right)}{a_0\left((e^{a_0\varsigma})^4b_0-4a_0\sin(b_0\varsigma)\cos(b_0\varsigma)(e^{a_0\varsigma})^2-b_0\right)}$$

749 $$C_4(\varsigma)=\frac{e^{a_0\varsigma}}{2}\frac{-3a_0^2\cos(b_0\varsigma)b_0+2a_0^3\sin(b_0\varsigma)-b_0^3\cos(b_0\varsigma)+(e^{a_0\varsigma})^2\left(2a_0b_0^2\sin(b_0\varsigma)-a_0^2b_0\cos(b_0\varsigma)+b_0^3\cos(b_0\varsigma)\right)}{a_0b_0\left((e^{a_0\varsigma})^4b_0-4a_0\sin(b_0\varsigma)\cos(b_0\varsigma)(e^{a_0\varsigma})^2-b_0\right)}$$

750 $$\varsigma=e-\xi$$